Note: This copy is for your personal, non-commercial use only. To order presentation-ready copies for distribution to your colleagues or clients, contact us at www.rsna.org/rsnarights.

Prostate Cancer: Multiparametric MR Imaging for Detection, Localization, and Staging[1]

Caroline M. A. Hoeks, MD
Jelle O. Barentsz, MD, PhD
Thomas Hambrock, MD
Derya Yakar, MD
Diederik M. Somford, MD
Stijn W. T. P. J. Heijmink, MD
Tom W. J. Scheenen, PhD
Pieter C. Vos, MSc
Henkjan Huisman, MSEE, PhD
Inge M. van Oort, MD, PhD
J. Alfred Witjes, MD, PhD
Arend Heerschap, PhD
Jurgen J. Fütterer, MD, PhD

This review presents the current state of the art regarding multiparametric magnetic resonance (MR) imaging of prostate cancer. Technical requirements and clinical indications for the use of multiparametric MR imaging in detection, localization, characterization, staging, biopsy guidance, and active surveillance of prostate cancer are discussed. Although reported accuracies of the separate and combined multiparametric MR imaging techniques vary for diverse clinical prostate cancer indications, multiparametric MR imaging of the prostate has shown promising results and may be of additional value in prostate cancer localization and local staging. Consensus on which technical approaches (field strengths, sequences, use of an endorectal coil) and combination of multiparametric MR imaging techniques should be used for specific clinical indications remains a challenge. Because guidelines are currently lacking, suggestions for a general minimal protocol for multiparametric MR imaging of the prostate based on the literature and the authors' experience are presented. Computer programs that allow evaluation of the various components of a multiparametric MR imaging examination in one view should be developed. In this way, an integrated interpretation of anatomic and functional MR imaging techniques in a multiparametric MR imaging examination is possible. Education and experience of specialist radiologists are essential for correct interpretation of multiparametric prostate MR imaging findings. Supportive techniques, such as computer-aided diagnosis are needed to obtain a fast, cost-effective, easy, and more reproducible prostate cancer diagnosis out of more and more complex multiparametric MR imaging data.

© RSNA, 2011

Online CME

See www.rsna.org/ry_cme.html

Learning Objectives:

- Recognize prerequisites, analytic methods, artifacts, and important considerations for acquisition and evaluation of prostate functional MR imaging techniques such as dynamic contrast-enhanced MR imaging, diffusion-weighted MR imaging, and proton MR spectroscopy.
- Identify required multiparametric MR imaging techniques needed for evaluation for different clinical indications for prostate MR imaging.

Accreditation and Designation Statement

The RSNA is accredited by the Accreditation Council for Continuing Medical Education (ACCME) to provide continuing medical education for physicians. The RSNA designates this journal-based activity for a maximum of 1.0 *AMA PRA Category 1 Credit*™. Physicians should claim only the credit commensurate with the extent of their participation in the activity.

Disclosure Statement

The ACCME requires that the RSNA, as an accredited provider of CME, obtain signed disclosure statements from the authors, editors, and reviewers for this activity. For this journal-based CME activity, author disclosures are listed at the end of this article. The editor and the reviewers indicated that they had no relevant relationships to disclose.

[1] From the Departments of Radiology (C.M.A.H., J.O.B., T.H., D.Y., S.W.T.P.J.H., T.W.J.S., P.C.V., H.H., A.H., J.J.F.) and Urology (D.M.S., I.M.v.O., J.A.W.), Radboud University Nijmegen Medical Centre, Geert Grooteplein zuid 10, NL 6500 HB, Nijmegen, the Netherlands; and Department of Urology, Canisius Wilhelmina Hospital, Nijmegen, the Netherlands (D.M.S.). Received October 14, 2009; revision requested December 16; revision received July 5, 2010; accepted August 27; final version accepted January 14, 2011; final review by C.M.A.H June 1. Supported by the Dutch Cancer Society. **Address correspondence to** C.M.A.H. (e-mail: *C.Hoeks@rad.umcn.nl*).

© RSNA, 2011

The most recent estimation by the International Agency for Research on Cancer revealed 679 000 new cases of and 221 000 deaths related to prostate cancer on a global level in 2002 (1). With an estimated 5-year prevalence of 2.3 million patients in the world, prostate cancer is a major global health problem.

Essentials

- Multiparametric MR imaging of the prostate consists of the combination of T1- and T2-weighted anatomic imaging and functional MR techniques, including diffusion-weighted (DW) imaging, dynamic contrast-enhanced imaging, and MR spectroscopic imaging.
- Guidelines on the optimal imaging protocols and combinations of multiparametric MR imaging techniques for different clinical prostate cancer indications are an important necessity, yet they are lacking.
- A suggestion for minimal requirements for multiparametric MR imaging is a combination of T1- and T2-weighted imaging with DW or dynamic contrast-enhanced MR imaging; for detection and localization, the use of a pelvic phased-array coil is sufficient, but for staging use of an endorectal coil is preferred.
- Although reported accuracies of different components of multiparametric MR imaging techniques are inconsistent, in general the addition of multiparametric MR imaging techniques to T2-weighted MR imaging improves accuracy for both localization and local staging of prostate cancer.
- Of all clinical indications for multiparametric MR imaging of the prostate, localization is the most important: Accurate localization of prostate cancer results in more accurate prostate cancer staging and MR guidance of prostate biopsy and therapy.

Prostate cancer diagnostics are initiated on the basis of prostate-specific antigen (PSA) measurements and determination of clinical stage by means of digital rectal examination. Definite diagnosis is usually obtained by means of transrectal ultrasonography (US)-guided systematic random prostate biopsies. Histopathologic analysis of these biopsy samples provides the clinician with information on the Gleason score. This is a histopathologic score that correlates with prostate cancer prognosis (2,3).

Nomograms (4) based on the combination of PSA level, digital rectal examination findings, and systematic random biopsy–based Gleason score are used to determine the choice of therapy and prognosis. However, each of these tests has its shortcomings: Digital rectal examination has a low overall sensitivity (37%) and low positive predictive value when lower PSA ranges of 0–3 ng/mL are encountered (5). PSA measurement has yielded higher detection rates than has digital rectal examination (6), but its specificity is low (36%) owing to false-positive PSA elevation under benign circumstances, such as inflammation or benign prostatic hyperplasia (BPH) (7). When digital rectal examination results are positive or when the PSA level is elevated, systematic random sextant biopsy with acquisition of a minimum of four extra cores from lateral peripheral zones or from a region that is suspicious for cancer is generally recommended to be performed initially (8). Systematic random biopsy is prone to undersampling (35% cancers missed on first biopsy [9] and underestimation Gleason grade in 46% of cases [10]). These inaccurate tools often lead to incorrect diagnoses, inaccurate risk assessments, and less optimal therapy choices. Because these diagnostic methods all have their limitations, there is a need for improved prostate cancer diagnosis with improved detection, localization, and sampling.

In the mid 1980s, the first prostate magnetic resonance (MR) imaging examinations were performed. Since then, MR imaging has evolved from a promising technique into a mature prostate imaging modality (11,12). MR imaging can provide functional tissue information along with anatomic information. To increase the accuracy, anatomic T2-weighted MR imaging and functional MR imaging techniques such as dynamic contrast agent–enhanced MR imaging, diffusion-weighted (DW) imaging, and hydrogen 1 MR spectroscopic imaging should be combined in an integrated multiparametric MR imaging examination. These multiparametric MR techniques will contribute to prostate cancer diagnostics, although results for detection, localization, and local staging of prostate cancer vary greatly among the studies performed.

This article will describe the fundamentals of multiparametric MR imaging of prostate cancer. We will provide an overview of the individual MR imaging techniques with their combined merits and limitations for clinical challenges such as detection, localization, local staging, and active surveillance of prostate cancer.

MR Imaging Techniques

Anatomic T2-weighted MR Imaging

T2-weighted MR imaging is the workhorse of prostate MR imaging. T2-weighted MR images have high spatial resolution and, thus, can clearly differentiate the normal intermediate- to high-signal-intensity peripheral zone from the low-signal-intensity central and transition zones in young male subjects (13). In the aging man, owing to variable extension of the transition zone due to BPH, the size and signal intensity

Published online
10.1148/radiol.11091822 **Content codes:** GU MR MA

Radiology 2011; 261:46–66

Abbreviations:
ADC = apparent diffusion coefficient
A_z = area under the receiver operating characteristic curve
BPH = benign prostatic hyperplasia
DW = diffusion weighted
K^{trans} = volume transfer constant
PSA = prostate-specific antigen

Potential conflicts of interest are listed at the end of this article.

of the prostate transition zone may vary. BPH itself is a round, well-defined, inhomogeneous area with (variable) intermediate signal intensity and a low-signal-intensity rim that surrounds the expanded transition zone (12). Because of transition zone expansion, the remainder of the compressed central zone is often indefinable on MR images.

High-spatial-resolution T2-weighted rapid acquisition with refocused echo sequences with a small field of view, performed with endorectal and/or external body phased-array coils, are generally used to depict prostate anatomy. T1-weighted contrast in the prostate is very low. Therefore, it is not possible to appreciate the different anatomic zones on T1-weighted images. On T2-weighted images, prostate cancer can appear as an area of low signal intensity within the high signal intensity of a normal peripheral zone. An example of this finding is shown In Figure 1a. The degree of signal intensity decrease may differ with the Gleason score: Higher Gleason score components 4 or 5 have shown lower signal intensities than do lower Gleason score components 2 and 3 (14). The density and the growth pattern of the cancer may also influence T2-weighted signal intensity. Cancers in the peripheral zone, which grow thinly scattered into the surrounding normal tissue, have shown no significant difference in quantitative T2 values with normal peripheral zone. On the other hand, densely growing cancers do show lower quantitative T2 values (15).

A limitation of T2-weighted imaging is that focal areas of low signal intensity in the peripheral zone do not always represent cancer. Benign abnormalities such as chronic prostatitis, atrophy, scars, postirradiation or hormonal treatment effects, hyperplasia, and postbiopsy hemorrhage may mimic tumor tissue (16). Low-signal-intensity lesions with a wedge shape and a diffuse extension without mass may be reliable signs of benignity (17). Hemorrhage may be differentiated on the basis of its high signal intensity on T1-weighted images. When methemoglobin is present in hemorrhagic regions, its paramagnetic characteristics result in high signal intensity on T1-weighted MR images. Preferably, MR imaging of patients suspected of having prostate cancer should be avoided for 8 weeks after prostate biopsy to allow reduction of artifacts due to postbiopsy hemorrhage (18).

Owing to the presence of BPH, cancer in central and transition zones is more difficult to discern. BPH may have signal intensity similar to that of prostate cancer on T2-weighted images. However, it has been reported that features such as homogeneously low T2-weighted signal intensity (Fig 1b), ill-defined irregular edges of the suspicious lesion, invasion into the urethra or the anterior fibromuscular stroma (Fig 1b), and lenticular shape are helpful signs for detection of malignancy in the transition zone (19).

Combined T1-weighted and T2-weighted MR imaging should be used for all clinical prostate cancer indications to evaluate anatomy and possible postbiopsy hematoma artifacts.

Dynamic Contrast-enhanced MR Imaging

Angiogenesis in prostate cancer tissue is induced by secretion of vascular growth factors in reaction to the presence of local hypoxia or lack of nutrients (20). Resultant changes in vascular characteristics can be studied well with dynamic contrast-enhanced MR imaging (Fig 2). This technique exploits the dynamic uptake and rapid washout of a gadolinium chelate contrast agent to show the typical pharmacokinetics of cancerous tissue. Because the prostate as a whole is highly vascularized, a simple comparison of pre- and postgadolinium images is usually insufficient to discern prostate cancer (21,22).

A fast and direct method to characterize prostatic vascular pharmacokinetic features is high-temporal-resolution dynamic contrast-enhanced MR imaging. Dynamic contrast-enhanced MR imaging consists of a series of fast T1-weighted sequences covering the entire prostate before and after rapid injection (2–4 mL/sec) of a bolus of a low-molecular-weight gadolinium chelate such as gadoterate meglumine or gadopentetate dimeglumine (concentration, 0.1–0.2 mmol/kg) (23,24). In addition to the most frequently used fast sequences, which have a high temporal resolution (a short period of 1–4 seconds between measurements), slow sequences (temporal resolution, 30 seconds with higher spatial resolution) have also been used.

Depending on the area of anatomic coverage, the acquisition times, potential susceptibility artifacts, and desired T1 sensitivity, a choice for a faster or slower sequence must be made (25). On one hand, fast sequences may improve tissue characterization because the prostate enhances quickly with T1-weighted dynamic contrast-enhanced MR sequences. With fast sequences, accurate quantification of different pharmacokinetic enhancement parameters is possible. On the other hand, fast T1-weighted sequences have trade-offs, including reduced spatial resolution and/or anatomic coverage. Optimal spatial and temporal resolutions based on clinical indications remain subjects of future research.

Prior to postprocessing of dynamic contrast-enhanced MR imaging data, estimation of the arterial input function can be performed. In the Tofts model, the arterial input function can be calculated with a formula that uses values of plasma concentration after administration of a bolus in healthy subjects (26). In addition to the Tofts model, automatic derivation of the arterial input function from reference tissues can be performed (27). The latter method has the advantages that it needs only T1-weighted MR images and that the arterial input function is estimated accurately in a large reference tissue volume.

Assessment of signal intensity changes on T1-weighted dynamic contrast-enhanced MR images in order to estimate contrast agent uptake in vivo can be performed qualitatively, semiquantitatively or quantitatively. Qualitative analysis of signal intensity changes can be achieved by assessing the shape of the signal intensity–time curve. Quantification of signal intensity changes, which are generally represented by gadolinium concentration–time curves, requires semiquantitative

Figure 1

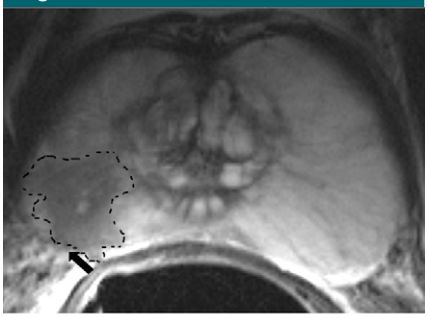

a.

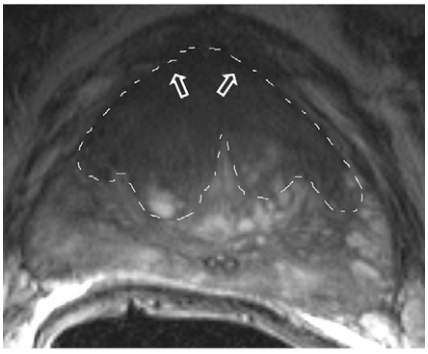

b.

Figure 1: Axial T2-weighted turbo spin-echo MR images (repetition time msec/echo time msec, 4260/99; flip angle 120°) of prostate cancer. **(a)** At level of midprostate to apex, a low-signal-intensity lesion is present on the right side of the prostate, within the high signal intensity of the peripheral zone (outline), with signs of minimal capsular invasion (arrow). At prostatectomy, this lesion, which was suspicious for prostate cancer, corresponded to stage T3a (extracapsular extension of 5 mm), Gleason score 7 (4+3) prostate cancer. **(b)** At midprostate level, a homogeneous low signal intensity area in the ventral transition zone is seen (outline), with loss of visibility of healthy BPH structures ("charcoal sign"). Invasion of anterior fibromuscular stroma at the ventral prostate can be seen (arrows). This lesion was suspicious for transition zone cancer. At prostatectomy, stage T2c, Gleason score 6 (2+4) prostate cancer was found.

assessment of contrast agent concentration or calculation of different quantitative physiologic parameters by using pharmacokinetic compartmental modeling. Washout is a semiquantitative parameter that captures the curve pattern after the first peak of enhancement. Other semiquantitative parameters are *(a)* integral area under the gadolinium-concentration–time curves, *(b)* wash-in gradient (upward slope of first pass), maximum signal intensity, *(c)* time-to-peak enhancement, and *(d)* start of enhancement. Semiquantitative parameters have the advantages of being fast, relatively simple to calculate, and of being available on current MR systems. They may, however, be influenced by MR unit settings (22).

In quantitative pharmacokinetic analysis, the behavior of a volume of contrast agent in the intravascular space versus that in the extravascular extracellular space is estimated in volume units for a certain period of time. The return of the contrast agent to the extracellular extravascular space can be limited by flow, by permeability of the endothelium, or by a combination of flow and endothelium permeability. The flow-limited Kety model (28), the permeability-limited Tofts model (29) and mixed models (30,31) are applicable under these respective circumstances. Tofts et al (32) suggested the following standard pharmacokinetic quantitative parameters: V_e, which represents the volume fraction of extravascular extracellular leakage space and k_{ep}, which represents the exchange rate constant of contrast agent between the extracellular extravascular leakage space and the blood plasma (in units per minute). V_e and k_{ep} are related with the following equation in the Tofts model: $k_{ep} = K^{trans}/V_e$. When flow is limited, the volume transfer constant K^{trans} equals the blood plasma flow per unit volume of tissue. Under permeability-limited, conditions, K^{trans} equals the permeability surface area product per unit volume of tissue, which is the case in prostate cancer. Prostate cancer tends to enhance earlier, faster, and to a greater extent and shows earlier contrast agent washout, as compared with healthy prostate tissue (23,33). This characteristic makes dynamic contrast-enhanced MR imaging a sensitive technique for prostate cancer localization. Estimated quantitative parameters can be presented to the radiologist as color-overlay maps on anatomic T2-weighted MR images to relate dynamic contrast-enhanced MR images to prostate anatomy. Prostate cancer diagnostics for clinical indications such as local staging can then be improved by better prostate cancer localization characteristics obtained with dynamic contrast-enhanced MR imaging. This advantage will be addressed in the Clinical Questions section.

One of the limitations of dynamic contrast-enhanced MR imaging is related to discrimination of cancer from prostatitis in the peripheral zone and from highly vascularized BPH nodules in the transition zone (34). Other shortcomings are a limited use of standardized approaches for calibration and analysis, the shortage of uniform commercially available tools for pharmacokinetic analysis, and the lack of consensus in acquisition protocols.

Correlation of dynamic contrast-enhanced MR images with prognostic histopathologic markers of prostate cancer angiogenesis has rarely been performed. This remains an important area for future research (35).

Dynamic contrast-enhanced MR imaging is an accurate functional MR imaging technique that can be used for all clinical indications discussed in this article. In a multiparametric MR imaging examination, the high sensitivity of dynamic contrast-enhanced MR may be used for initial evaluation of potential tumor locations. Other functional MR imaging techniques may subsequently be added to increase specificity for prostate cancer localization, because sensitivity of dynamic contrast-enhanced MR imaging is low. Little standardization exists in acquisition protocols and analytic models for dynamic contrast-enhanced MR imaging.

DW Imaging

In DW imaging, proton diffusion properties in water are used to produce image contrast. Images that reflect proton diffusion are acquired by applying motion-encoding gradients, which cause phase shifts in moving protons, depending on the direction and quantity of their movement (36). The attenuation of the MR signal in DW imaging is expressed with the Stejskal-Tanner equation (36). The *b* value and the apparent diffusion coefficient (ADC) are components in

Figure 2

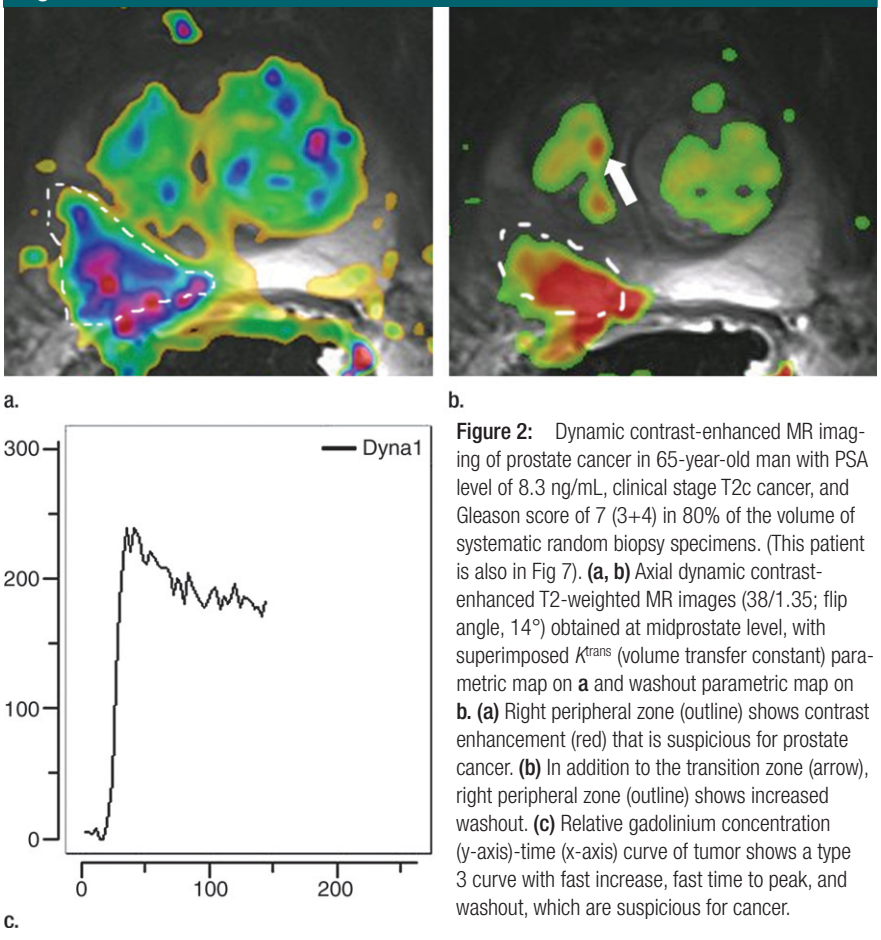

Figure 2: Dynamic contrast-enhanced MR imaging of prostate cancer in 65-year-old man with PSA level of 8.3 ng/mL, clinical stage T2c cancer, and Gleason score of 7 (3+4) in 80% of the volume of systematic random biopsy specimens. (This patient is also in Fig 7). **(a, b)** Axial dynamic contrast-enhanced T2-weighted MR images (38/1.35; flip angle, 14°) obtained at midprostate level, with superimposed K^{trans} (volume transfer constant) parametric map on **a** and washout parametric map on **b. (a)** Right peripheral zone (outline) shows contrast enhancement (red) that is suspicious for prostate cancer. **(b)** In addition to the transition zone (arrow), right peripheral zone (outline) shows increased washout. **(c)** Relative gadolinium concentration (y-axis)-time (x-axis) curve of tumor shows a type 3 curve with fast increase, fast time to peak, and washout, which are suspicious for cancer.

this equation. While the *b* value expresses the amount of diffusion weighting, ADC reflects the movement of the water molecules within the interpulse time. Because ADC quantifies the flow as well as the distance a water molecule has moved, it represents both capillary perfusion and diffusion characteristics (37). Fitting the Stejskal-Tanner equation for every pixel on two or more DW images acquired with different *b* values results in an ADC map. For prostate cancer, DW imaging *b* values between 500 and 800 sec/mm^2 are typically used (38). *b* Values of 1000 and even 2000 sec/mm^2 may increase the accuracy of prostate cancer detection (39). Especially within the transition zone, high *b* values may help improve differentiation of BPH from prostate cancer (40).

Healthy prostate tissue in the peripheral zone, which is rich in tubular structures, allows extensive diffusion of water molecules within the gland tubules. Consequently, ADCs in healthy peripheral zone tissues can be high. Prostate cancer tissue destroys the normal glandular structure of the prostate and replaces ducts. It also has a higher cellular density than does healthy prostate peripheral zone tissue (38). On ADC maps, therefore, prostate cancer often shows lower ADCs in comparison to surrounding healthy peripheral zone prostate tissue (41). Examples of this are presented in Figure 3. Recently, 3 T DW imaging ADCs were shown to correlate significantly with the cellular density of prostate cancer in radical prostatectomy specimens (42).

Because the acquired ADC depend on the specific pulse sequence parameters (especially the *b* values), the specific MR systems used, and the magnetic field strength, the ADCs of healthy and cancerous tissue have varied among reported studies. Furthermore, there is an overlap in the ADCs of healthy tissue and those of prostate cancer, within and between subjects, which limits the determination of a single threshold ADC for malignancy (43).

Mean ADCs for prostate cancer versus those for healthy prostate tissue obtained at different field strengths, with or without the use of an endorectal coil in different anatomic regions are shown in Table 1. Owing to variation in ADCs of benign prostate tissue in the peripheral and transition zones, the area under the receiver operating characteristic curve (AUC) for differentiation of prostate cancer from benign tissue can vary by anatomic location within the prostate gland and are found to be lower in the prostatic base (AUC of 0.725 in prostate base vs 0.952 and 0.906 for overall peripheral and transition zones, respectively) (44). The reported differences in detection accuracies with DW imaging might be explained by the different tissue composition in different anatomic zones of the prostate. It has been hypothesized that a higher degree of proton motion in the extracellular water compartment occurs as opposed to that in intracellular water, where movement is restricted by cell membranes or other intracellular structures (38). As a result of variation in glandular tissue within a healthy peripheral zone to muscular or fibrous tissue within the transition zone, the ratio of intracellular versus extracellular water also differs. This variation might also explain the variability of ADCs in healthy prostate tissue that have been reported. Relative ADC thresholds calibrated to an individual gray-scale value may be a way to overcome intra- and interindividual variation and overlap of ADCs of cancer and healthy prostate tissue (45).

DW imaging is a fast, simple, and readily available MR imaging technique for prostate cancer. Nevertheless, DW imaging of the prostate has the limitation of low in-plane spatial resolution, even at 3 T. Consequently, DW imaging is not a preferred technique for

Figure 3

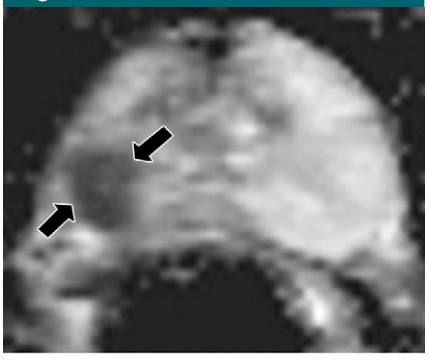

a.

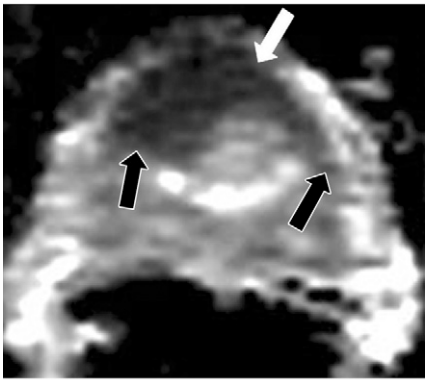

b.

Figure 3: DW imaging of prostate cancer. Axial ADC maps (2400/81; $b = 0, 50, 500$ and 800 sec/mm^2) obtained at midprostate level in same patients as in Figure 1a (**a**) and 1b (**b**). **(a)** Lesion with low ADC (mean ADC = 0.8×10^{-3} mm^2/sec), is suspicious for cancer in right peripheral zone (arrows). This indicates intermediate to high cancer aggressiveness. At prostatectomy, the lesion was determined to be stage T3a, Gleason score 7 (4+3) prostate cancer. **(b)** Comma-shaped area with low ADC (mean ADC = 0.6×10^{-3} mm^2/sec) is seen in ventral transition zone (arrows). This indicates intermediate to high cancer aggressiveness. At prostatectomy, lesion was determined to be stage T2c, Gleason score 6 (2+4) prostate cancer.

prostate cancer staging. However, DW imaging does reflect cellular density, which makes the technique potentially suitable to determine tumor aggressiveness. DW imaging, being a technique for measuring proton motion, is very sensitive to motion artifacts. Single-shot echo-planar MR imaging is used to decrease motion artifacts by acquiring images in less than 1 second. Because the phase-encoding bandwidth per pixel is very small, echo-planar imaging is very sensitive to magnetic field inhomogeneities. As a result, artifacts occur in areas with large variations in magnetic susceptibility, such as in tissue-air interfaces (air in the rectum or endorectal coil) or in chemical shift in areas with water-fat interfaces. Parallel imaging and short-imaging-time protocols are used to overcome these off-resonance artifacts (46).

Correlation of DW imaging results and histopathologic findings as well as to prognostic histologic prostate cancer markers such hypoxia-inducible factors, should be another area for future research.

Of all functional MR imaging techniques DW imaging is the most practical and simple in its use. Within a multiparametric MR imaging examination DW imaging may be used for all clinical indications discussed in this article. DW imaging has the disadavantages of being susceptible to motion and to magnetic field inhomogeneities.

Proton MR Spectroscopic Imaging

In MR spectroscopic imaging, spectral profiles are measured in two or three spatial dimensions. These spectral profiles reflect resonance frequencies that are unique for protons in different metabolites present at the sampled location. The specific resonance frequencies or chemical shifts are given relative to a reference frequency in parts per million (ppm). In human prostate examinations, MR spectroscopic imaging is usually performed in a volume that covers the whole prostate, which is subdivided up into a three-dimensional grid of multiple voxels. With the introduction of the endorectal coil for prostate MR examinations, it became possible to obtain in vivo MR spectroscopic imaging spectra of small voxels in the prostate (less than 1 cm^3) with sufficient signal to noise (47–49). The dominant peaks observed in these spectra are from protons in citrate (approximately 2.60 ppm), creatine (3.04 ppm) and choline compounds (approximately 3.20 ppm). Polyamine signals (mostly from spermine) also may be observed (approximately 3.15 ppm) at various relative intensities, depending on the acquisition conditions. Compared with healthy peripheral tissue or BPH tissue, citrate signals are reduced and those of choline compounds are often increased in prostate cancer tissue (Fig 4) (50). Citrate is produced in epithelial cells as an intermediate product in the Krebs cycle due to aconitase inhibition. It then accumulates in the luminal space of the prostate. The lower citrate peak in cancer tissue may thus be caused by altered metabolism, as well as by a reduction of luminal space, which commonly occur in prostate cancer. Choline compounds are involved in the biosynthesis and degradation of phospholipids, which are required for the build-up and maintenance of cell membranes. An increased cell-turnover in prostate cancer results in an increased concentration of free choline-containing molecules within the cytosol and the prostate interstitial tissue.

Because differentiation of choline peaks from creatine peaks on spectra obtained at common clinical field strengths is often hampered by their bandwidths and by weaker signals from polyamines between them, the choline plus creatine–to-citrate ratio is mostly used as a metabolic biomarker for prostate cancer. An example of this is presented in Figure 4. In the analysis of patient data, it should be taken into account that different anatomic zones of the healthy prostate have different amplitudes for citrate, creatine, and choline, which are reflected in different choline plus creatine–to-citrate ratios. High citrate concentrations are found in the glandular tissues of the prostate such as the peripheral zone, which contains epithelial cells and secretory ducts. Therefore, citrate concentrations are highest in the peripheral zone and lower in the central zone. In the transition zone, the citrate concentration may be higher in case of glandular proliferation and lower in the case of stromal proliferation (51). Furthermore, because of the sensitivity profile of the surface coil, the spectral signal intensity will drop the farther away the tissue is from the ERC. Since the prostate is relatively small and embedded in adipose tissue,

Table 1

Mean ADCs for Prostate Zones at Different Field Strengths with or without an Endorectal Coil

	Peripheral Zone ADC		Transition Zone ADC	
Magnetic Field Strength (T)	Healthy Tissue ($\times 10^{-3}$ mm^2/sec)	Prostate Cancer ($\times 10^{-3}$ mm^2/sec)	Healthy Tissue ($\times 10^{-3}$ mm^2/sec)	Prostate Cancer ($\times 10^{-3}$ mm^2/sec)
1.5				
Without ERC	1.72–1.85 (79,133–135)	0.96–1.02 (79,133–135)	1.34–1.85 (79,133–135)	0.93–0.96 (79,133–135)
With ERC	1.51–1.69 (136,137)	1.39 (136)	1.31 (137)	–
3.0	1.86–2.61 (39,138,139)	1.19–1.38 (39,138,139)	1.77 (39,138,139)	1.21 (39)

Numbers in parentheses are reference numbers. ERC = endorectal coil.

much effort has been put into suppressing spectral contamination, not only of the high water signal, but also of strong lipid signals. Therefore, radiofrequency pulse schemes that selectively invert and dephase water and lipid signals have been developed (52,53). Frequency-selective suppression methods, such as Mescher-Garwood (or MEGA) pulses (52) or later band selective inversion with gradient dephasing (or BASING) are generally applicable because no high-performance gradients are necessary. Spectral-spatial pulses have the advantage of increased bandwidth, which results in decreased chemical shift–dependent localization errors. Three-dimensional MR spectroscopic imaging sequences are currently preferred over two-dimensional sequences because of the possibility of complete coverage of the entire prostate gland (47,54). Three-dimensional acquisitions can be performed in approximately 10–15 minutes with a resolution as low as 0.4 cm^3 with sufficient signal-to-noise ratio at 1.5 T (54).

MR spectroscopic imaging has several limitations. Spectral quality depends on magnetic field homogeneity, which must be optimized for each patient by shimming. Considerable local magnetic field distortions may occur due to hemorrhage, which is why the examination should be performed with sufficient delay from the time of biopsy. The clinical performance of MR spectroscopic imaging of the prostate can be improved by optimizing field shimming or by means of correction procedures, in addition to better signal-to-noise ratio and chemical shift dispersion, by using stronger magnetic fields (55). Currently, the interpretation of MR spectroscopic imaging results requires special expertise and is time consuming. Automated measurement procedures, rapid display of examination results, and proper training of clinical users are important to transform MR spectroscopic imaging into a practical and widespread clinical tool. To this day, these requirements are generally not met.

MR spectroscopic imaging is an accurate technique that may be used for all clinical indications mentioned in this article. MR spectroscopic imaging needs, however, relatively more time and expertise than do other functional MR imaging techniques, which limits its clinical applicability.

Combined Multiparametric MR Imaging

Because the functional MR imaging techniques we have discussed all have their strengths and shortcomings, they are combined in a multiparametric MR imaging prostate examination to increase accuracy. A multiparametric MR imaging prostate examination consists of T1- and T2-weighted imaging combined with one or more functional MR imaging techniques.

Within the variety of possible MR imaging protocols and combinations of different techniques, consensus guidelines are needed to increase accuracy and unity in the field (56). Because formal practice guidelines for multiparametric prostate imaging are currently unavailable, the following suggestions for possible prostate multiparametric MR imaging protocols for different clinical indications can be recommended. Patients with a clinical indication of prostate cancer detection, who often have previously undergone one or more systematic random biopsies with negative results, may have a high a priori risk for transition zone cancer (57). In these patients, it is essential not only to use techniques such as T2-weighted and dynamic contrast-enhanced MR imaging, which may yield false-positive or false-negative results within the transition zone, but also DW imaging (with a high *b* value), which may be a valuable technique in difficult detection cases. In patients referred for pretreatment staging, it is important to use an endorectal coil in combination with anatomic T2-weighted MR imaging. Because accurate localization may improve accurate staging it may be important to add at least one multiparametric MR imaging technique (Fig 5). Patients with a clinical indication for active surveillance or focal therapy need evaluation of the stage of the cancer and its aggressiveness. Preferably, an endorectal coil could be used in combination with more than one multiparametric technique that yields findings related to prostate cancer Gleason score (DW imaging and/or MR spectroscopic imaging) (Fig 6).

The optimal strength of multiparametric MR imaging is achieved by combining the information obtained with the various techniques. Computer programs, which allow evaluation of two or more multiparametric images in one view, need to be developed for the integrated interpretation of anatomic and functional findings. An example of how this could be accomplished is presented in Figure 7. Development of supportive techniques like computer aided diagnosis (58–60) is needed to achieve fast and reproducible diagnostics from large quantities of complex data. Furthermore, the education, experience, and

Figure 4

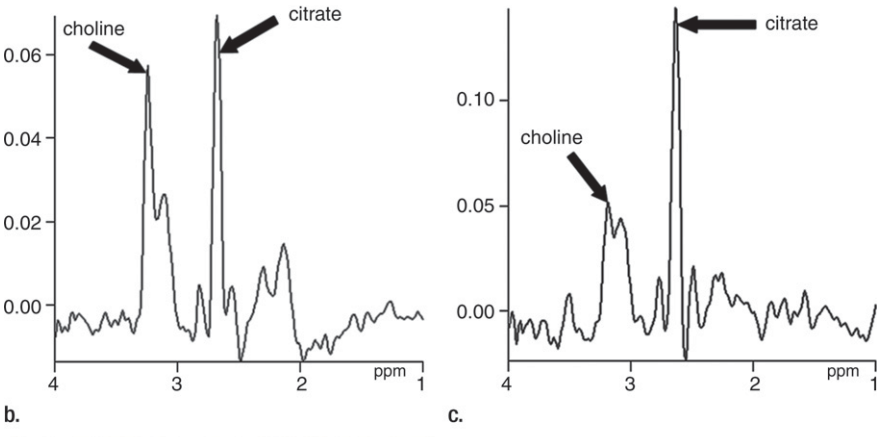

Figure 4: MR spectroscopic imaging in a 70-year-old man (same as in Fig 11) with a PSA level of 12 ng/mL and well-differentiated prostate cancer. (a) Axial T2-weighted turbo spin-echo MR image (4260/99; flip angle, 120°) shows stage T3a prostate cancer. Radical prostatectomy revealed a solitary Gleason score 7 (3+4) adenocarcinoma with extraprostatic extension. Red voxel has been placed in low-signal-intensity lesion in left peripheral zone, which is suspicious for cancer; blue voxel has been placed in benign-appearing region in right peripheral zone. **(b)** MR spectrum (750/145; flip angle, 90°) from red voxel shows choline peak that is increased relative to citrate peak. The choline plus creatine–to-citrate ratio, calculated from the integrals of the spectral peaks from choline, creatine, and citrate, is 0.80, which is suspicious for prostate cancer. **(c)** MR spectrum (750/145; flip angle, 90°) from blue voxel demonstrates low choline peak and high citrate peak, consistent with benign peripheral zone tissue. The choline plus creatine–to-citrate ratio is 0.32.

dedication of radiologists are essential for correct interpretation of findings from multiparametric MR imaging of the prostate (61).

Minimal requirements for a multiparametric MR imaging protocol include a combination of T1- and T2-weighted MR imaging with DW and dynamic contrast-enhanced MR imaging. For detection and localization indications, the use of a phased-array coil is sufficient; for staging indications, combination with an endorectal coil may be preferred.

MR Imaging–guided Biopsy

As mentioned earlier, systematic random biopsy is prone to sampling error, which often results in inaccurate prostate cancer detection and Gleason score grading (10). MR-guided prostate biopsy can potentially improve prostate cancer detection, because multiparametric MR imaging–guided biopsy can be targeted toward previously determined regions that are suspicious for cancer. MR-guided biopsy is technically feasible and can be performed on a routine basis (Fig 8). Owing to its limited availability and long examination time, this technique is typically used in patients with one or more previous negative systematic random biopsy sessions. Transrectal MR-guided biopsy performed at 1.5 T has shown promising cancer detection rates of 38%–59% (57,62–64). These detection rates are promising in comparison to those of systematic random biopsy rates of 22%–29% (9,65) after one session and 10%–17% after two sessions (9,65).

Use of multiparametric MR imaging in MR-guided biopsy planning has been studied by Franiel et al (66) in a prospective study of 1.5-T MR imaging in 54 patients with a median of two previous negative random systematic transrectal US-guided biopsies. Their ground truth was based on MR-guided biopsy of suspicious identifiable lesions from at least one multiparametric MR imaging technique only. They concluded that a combination of T2-weighted with DW MR imaging and either dynamic contrast-enhanced MR imaging or MR spectroscopic imaging reduced the number of areas that need to be subject to biopsy by 13%–15% while only missing 6% of cancers, in comparison to multiparametric MR imaging with all three techniques.

A limitation of MR-guided biopsy is that a multiparametric MR imaging and the MR-guided biopsy need to be performed in separate sessions because image postprocessing and exact tumor localization demand time. Another disadvantage is movement of the prostate during the biopsy procedure (67).

MR imaging findings have also been used to help direct biopsies under transrectal US guidance with reasonable to good detection rates of 25%–55% (68,69). Moreover, Gleason score concordance with radical prostatectomy findings may be improved with MR image guidance of transrectal US-guided prostate biopsy (70). Experimental fusion of MR and transrectal US data (71), in which distances between corresponding data points for each technique are rendered as small as possible by means of registration, is used to obtain more accurate MR-guided transrectal US prostate biopsy results (72).

Transrectal MR-guided biopsy improves prostate cancer detection; however, its availability is limited, and examination times are long. MR guidance of prostate biopsy is a very promising method to improve determination of the true pretreatment Gleason score.

Clinical Questions

Detection

As stated earlier, clinical prostate cancer detection is currently performed by using tools with limited accuracy. Because the specificity of PSA measurement is

Figure 5

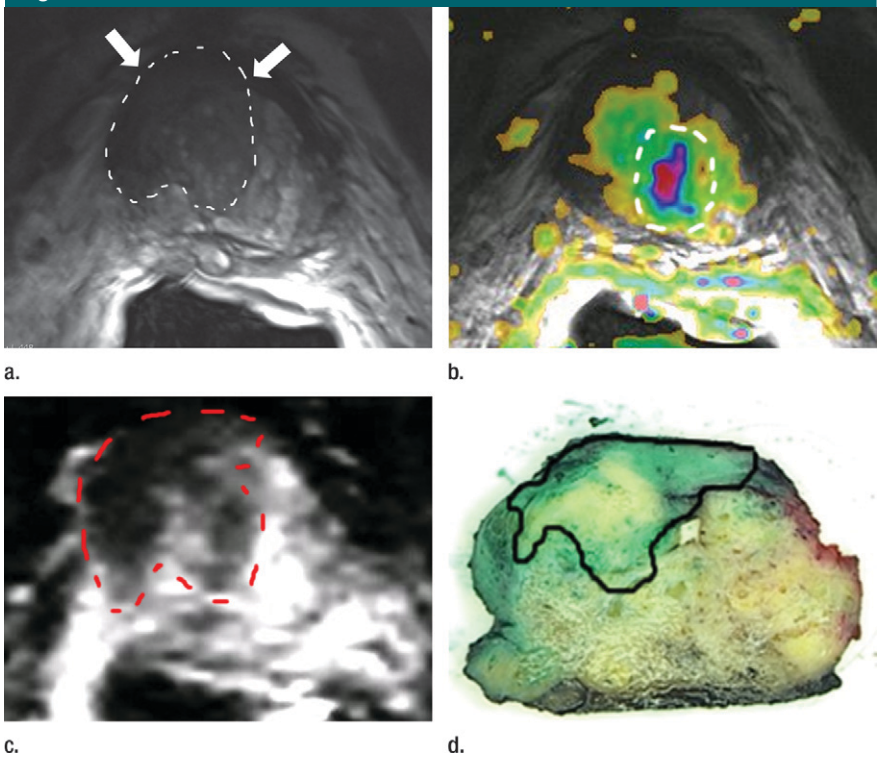

Figure 5: Multiparametric MR imaging for prostate cancer localization in the transition zone in a 67-year-old man with a PSA level of 17.6 ng/mL and Gleason score 7 prostate cancer shows the added value of multiparametric MR imaging for localization. While T2-weighted images yielded indeterminate findings for localization, and dynamic contrast-enhanced images yielded false-positive findings in another area, DW images were used to correctly localize this high-grade prostate cancer. **(a)** Axial T2-weighted turbo spin-echo image (4260/99; flip angle, 120°) obtained at the level of the base of the prostate shows area of lower signal in the right ventral prostate (outline), which is suspicious for prostate cancer. Bulging is present as a sign of stage T3 disease (arrows). **(b)** Axial MR image with superimposed K^{trans} parametric map (38/1.35; flip angle, 14°) at same level as **a.** Mediodorsal part of the prostate shows early enhancement (outline) but no increased K^{trans} at low-signal-intensity area in **a. (c)** On axial ADC map (2400/81; $b = 0, 50, 500, 800$ sec/mm^2) obtained at same level as **a,** the right ventral transition zone (outline) shows restriction (mean ADC = 606×10^{-6} mm^2/sec), which suggests highly aggressive cancer. **(d)** Axial whole-mount histopathologic slice from level corresponding to **a–c** shows stage T3b (Gleason score, 9 [4+5]) prostate cancer in right ventral prostate (outline).

low, it is often the case that many unnecessary repeat systematic random biopsies are required to establish a diagnosis (9).

Individual multiparametric MR imaging techniques such dynamic contrast-enhanced, DW and MR spectroscopic imaging have been shown (73–75) to be of possible additional value in prostate cancer detection (Fig 9). Because these MR techniques have a relatively high specificity in comparison with PSA measurement, they could prevent the unnecessary performance of systematic random biopsies and delay in diagnosis and treatment. Furthermore, results of prospective separate functional MR imaging studies for prostate cancer detection are difficult to compare, since criteria for cancer detection, methods of analysis, sample sizes, and mean PSA levels of patient groups differ or are not always presented.

It is essential to know if combinations of more than one functional MR technique could improve results even further. In a logistic regression analysis, ADC value was the best performing (area under the receiver operating characteristic curve [A_z] = 0.69) single parameter for prostate cancer detection when compared with T2-weighted imaging findings, K^{trans}, and extracellular extravascular space volume fraction v_e (73). In this study (73), a model based on T2-weighted MR imaging findings, ADCs, and K^{trans} performed best (A_z = 0.706). Although this study had a moderate sample size (n = 42) and was retrospective in character, it is one of the few prostate cancer detection studies in which prostatectomy specimens were used as the reference standard. In a recent evaluation of multiparametric MR imaging at 3 T (76), the addition of dynamic contrast-enhanced and/or DW imaging to T2-weighted MR imaging significantly improved prostate cancer detection sensitivity from 63% to 79%–81% in the peripheral zone, while maintaining a stable specificity. In the transition zone, however, multiparametric MR imaging did not improve prostate cancer detection. This study was performed in 57 patients, with prostatectomy specimens as ground truth. The combination of MR spectroscopic imaging with T2-weighted endorectal MR imaging has shown higher sensitivity (72%–89%) and equal specificity (79%–93%) for prostate cancer detection than was shown for anatomic MR imaging alone (sensitivity, 57%–84%; specificity, 50%–94%) (77,78).

Multiparametric MR imaging techniques may also contribute in detection of transition zone prostate cancers. The combined use of DW, dynamic contrast-enhanced, and T2-weighted MR imaging led to increased accuracy in detection of transition zone cancer, from 64% to 79%, in a small (n = 23) retrospective study (79).

Multiparametric MR imaging may potentially increase prostate cancer detection accuracy compared with the accuracy of T2-weighted MR imaging only. However, future research is needed to confirm initial results.

Localization and Local Staging

Prostate cancer localization is the most important clinical indication for multiparametric MR imaging of the prostate. First, accurate definition of prostate cancer location helps improve cancer

Figure 6

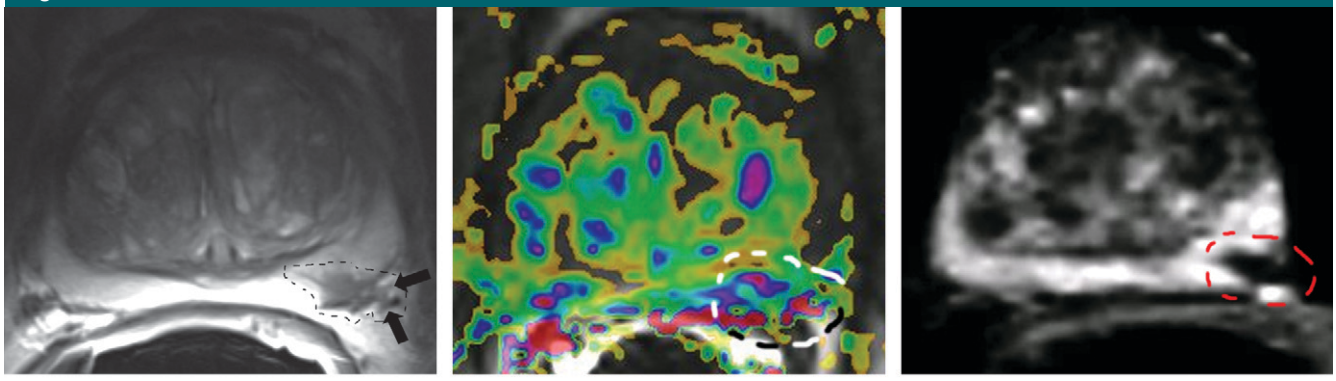

a. b. c.

Figure 6: Multiparametric MR imaging in a 69-year-old man undergoing active surveillance of Gleason score 6 (3+3) prostate cancer, found in 5% of the volume of one (left-sided) of nine systematic random biopsy core specimens. The patient had a PSA level of 6.7 ng/mL, PSA density of 0.9 ng/mL/mL, and clinical stage T2 disease. Multiparametric MR imaging findings obtained with an endorectal coil were suspect for stage T3a cancer in the left peripheral zone at the midprostate level. DW imaging findings indicated tumor intermediate to highly aggressive tumor at the same location. Subsequent MR-guided biopsy of this patient is depicted in Figure 8. **(a)** Axial T2-weighted turbo spin-echo MR image obtained with endorectal coil (4260/99; flip angle, 120°) at midprostate level shows small area of lower signal intensity in left peripheral zone (outline) with signs of extracapsular extension (arrows). **(b)** Axial MR image with superimposed K^{trans} parametric map (38/1.35; flip angle, 14°; same level as **a** and **b**) at the same level as **a**. Early enhancement occurs in multiple areas. The region suspicious for tumor is also enhanced (outline). **(c)** ADC map (2400/81; $b = 800$ sec/mm^2) shows restriction at the suspicious region in the left peripheral zone (outlined), indicating intermediate to highly aggressive tumor. Analysis of MR-guided biopsy specimen from the suspicious lesion resulted in Gleason score of 8 (3+5) in 80% of the specimen volume, with extension into periprostatic fat (stage T3a).

detection in targeting prostate biopsies with MR imaging guidance. Second, accurate definition of a prostate cancer location also helps improve prostate cancer staging, because better assessment of prostate cancer location(s) near the neurovascular bundle is possible in patients in whom nerve-sparing surgery is planned. Third, improved evaluation of prostate cancer location helps improve and support focused intensity-modulated radiation therapy planning of the dominant prostatic lesion and improves guidance of minimally invasive focal therapies.

In a large retrospective study in 106 patients in which prostatectomy findings were the reference standard (80), MR imaging localization of prostate cancer was significantly more accurate than digital rectal examination and systematic random biopsy results in the whole prostate except for the apex. Sensitivity and especially specificity of endorectal T2-weighted MR imaging prostate cancer localization vary, ranging from 54% to 91% and 27% to 91%, respectively (81–84). Variation of results in these prospective studies, in which prostatectomy findings served as reference standard, might be partially explained by the fact that image analysis was based on different numbers of regions of interest, different cutoff points for a positive result, and inclusion or exclusion of prostate cancer localization in the transition zone. Moreover, results vary as correlation of MR imaging findings with prostatectomy findings is difficult owing to different angles and section intervals of MR sections and prostatectomy slices and to deformation and shrinkage during histopathologic processing of the prostate specimens. Correction for this variability has been attempted by using a shrinkage factor (83,85). In a recent prospective study (84), correlation of MR imaging and prostatectomy findings was performed in an innovative and possibly more accurate way. Aside from dividing the prostate into 30 regions, including peripheral and transition zones, the authors also used an alternative-neighbor analytic approach to correct for prostate shrinkage and deformation. In this approach, tumors visible on MR image and seen in neighboring regions of the positive prostatectomy specimen were also considered to be positive MR results.

Localization merits of multiparametric MR imaging techniques may be used to draw the attention of the radiologist to a suspicious region. This is illustrated in Figures 5, 9, and 10.

Localization accuracy with dynamic contrast-enhanced MR imaging increased to 72%–91%, as compared with 69%–72% for anatomic T2-weighted MR imaging only (85–88). The addition of DW imaging (83) to T2-weighted MR imaging significantly improved sensitivity to 81% (sensitivity for T2-weighted MR imaging alone, 54%), whereas specificity was slightly lower for T2-weighted MR imaging combined with DWI (84%) than for T2-weighted MR imaging alone (91%) in this prospective prostatectomy-referenced study (83). Also, in other prospective studies (89,90), the addition of DW imaging to T2-weighted MR imaging improved prostate cancer localization performance, with A_z values of 0.66–0.79. However, in a recent retrospective 3-T study in 51 patients, with prostatectomy specimens as reference standard (91), DW imaging did not add value to T2-weighted MR imaging for prostate cancer localization. A_z values were 0.76–0.79 for T2-weighted

Figure 7

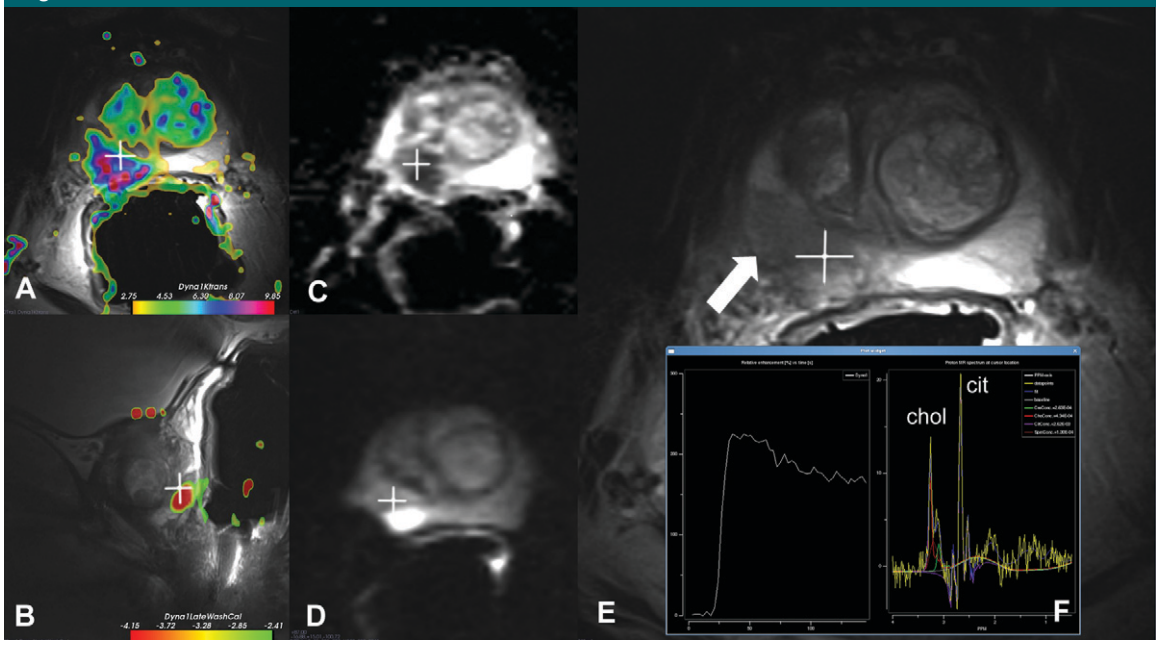

Figure 7: Multiparametric MR imaging of the prostate (same patient as in Fig 2: 65-year-old man, PSA level of 8.3 ng/mL, clinical stage T2c, Gleason score of 7 [3+4]) in screenshot generated by a computer-program, which can be used for image interpretation in multiparametric MR imaging. In addition to related views of multiplanar multiparametric images *(A–E),* quantitative information (*F)* is also displayed. *A–E* show tumor with bulging, suspicious for minimal stage T3A disease, in right peripheral zone at level of midprostate to apex (arrow). *A,* Axial K^{trans} map from dynamic contrast-enhanced MR imaging projected over T2-weighted image (see Fig 2 for parameters). *B,* Sagittal T2-weighted image (4290/98; flip angle, 120°) with color overlay showing washout (from dynamic contrast-enhanced MR imaging). *C,* Axial ADC map (2900/81; flip angle, 90°). *D,* Axial DW trace image (b = 800 sec/mm^2; 2900/81; flip angle, 90°). *E,* Axial T2-weighted image. *F,* Relative gadolinium concentration–time curve (left) and MR spectrum (right) from chosen point of interest in tumor (+). In MR spectrum, choline *(chol)* and citrate *(cit)* peaks can be evaluated. The low-signal-intensity lesion on *E* shows increased K^{trans} (on *A*), restriction on *C,* high signal intensity on *D,* gadolinium concentration–time curve type 3 and high choline peak on *F.* On a five-point scale, this can be scored 5/5 on T2-w, dynamic contrast-enhanced, DW, and MR spectroscopic images, for total score of 20/20, indicating intermediate to highly aggressive tumor.

MR imaging and 0.78–0.79 for T2-weighted MR imaging combined with DW imaging ADC maps. The high percentage of Gleason score 6 (3+3) cancers (36%, of which only 53%–63% were detected) may explain the poor incremental value of DW imaging ADC maps in this study.

MR spectroscopic imaging has shown higher specificity (68%–99%) and lower sensitivity (25%–80%) for prostate cancer localization, when compared with anatomic T2-weighted MR imaging (specificity, 61%–90%; sensitivity, 68%–87%) in prospective studies with prostatectomy specimens as reference standard (82,84,85,92). However, a multicenter trial that included 110 patients, with prostatectomy findings as reference standard (93), did not show any benefit for the addition of 1.5-T MR spectroscopic imaging to T2-weighted MR imaging in prostate cancer localization (A_z = 0.60 for T2-weighted MR imaging alone vs 0.58 for combined T2-weighted and MR spectroscopic imaging, P = .09). The omission of a multicenter validation and use of a threshold for increased metabolic ratios as a criterion for malignancy as well as of a clear definition of tumor focus size may have negatively influenced the quality of MR spectroscopic imaging in this trial. In a recent multiparametric 3-T MR imaging study with 57 patients (76), DW and dynamic contrast-enhanced MR imaging increased the accuracy of prostate cancer localization in the peripheral zone but failed to do the same in the transition zone. By using prostatectomy specimens as standard of reference and scoring four quadrants for both peripheral and transition zones, A_z values for the peripheral zone increased from 0.81 to 0.91–0.92 by adding DW and/or dynamic contrast-enhanced MR imaging to T2-weighted MR imaging. In the transition zone, however, localization accuracy decreased from A_z of 0.84 for T2-weighted MR imaging alone to 0.70–0.75 when dynamic contrast-enhanced imaging was added. With the addition of DW imaging to T2-weighted imaging, A_z values for cancer localization in the transition zone increased slightly from 0.84 to 0.88. By improving localization multiparametric MR imaging techniques may also contribute to improved local staging accuracy.

For appropriate therapy planning it is important to know if prostate cancer is confined to the gland (stages T1

Figure 8

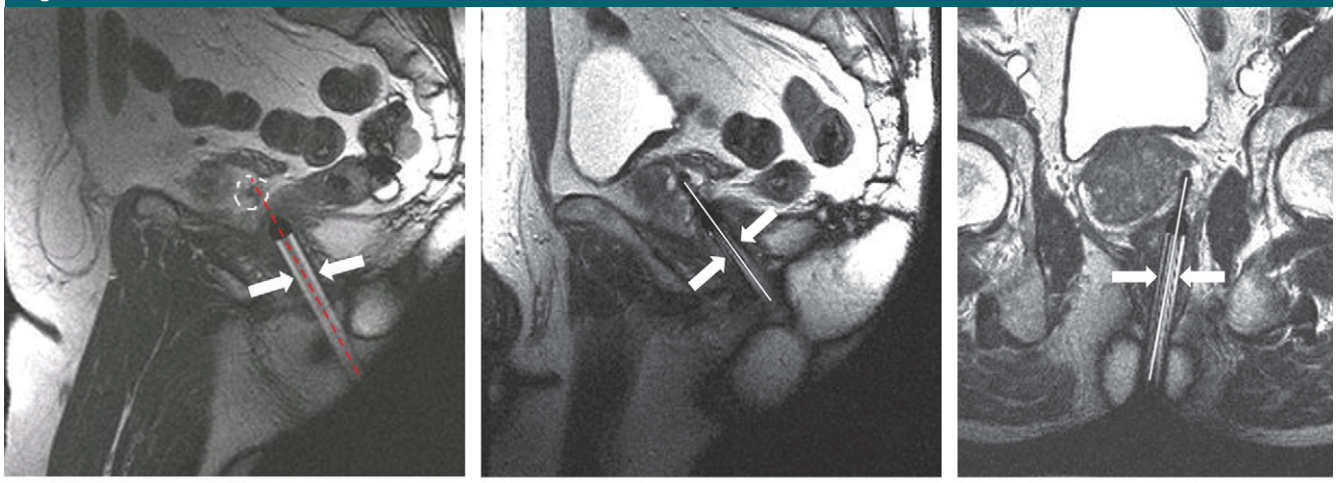

a. b. c.

Figure 8: **(a, b)** Sagittal and **(c)** axial gradient-echo MR images (4.48/2.24; flip angle, 70°) of MR-guided biopsy in a case of active surveillance of prostate cancer in a 69-year old man (same patient as in Fig 6) with Gleason score 6 (3+3) disease. Multiparametric staging MR imaging (not shown) with an endorectal coil resulted in suspicion of stage T3A cancer in left peripheral zone at midprostate. DW imaging (not shown) findings indicated intermediate to highly aggressive tumor in left peripheral zone. **(a)** Needle guide (arrows) is positioned toward target in left peripeheral zone at midprostate (outline). To accurately hit the target, the needle guide should be moved slightly caudad in sagittal plane; in position shown (red line), needle will miss the target. **(b, c)** Needle guide (arrows) is now accurately positioned and biopsy needle (line) has been inserted. MR guided biopsy of this suspicious lesion resulted in a Gleason score of 8 (3+5) for a volume percentage of 80% with extension into periprostatic fat (stage T3A). This patient was subsequently excluded from the active surveillance protocol.

and T2) or if there is extraprostatic extension (stages T3 and T4) (94). Current clinical staging, generally based on digital rectal examination, PSA and transrectal US findings, results in frequent understaging (59%) and some overstaging (5%) (95).

The main application of T2-weighted MR imaging is in local staging of prostate cancer. The most widely used criteria for extracapsular spread are (asymmetric) low signal intensity in the seminal vesicles, asymmetry of the neurovascular bundle, obliteration of the rectoprostatic angle (Fig 11), irregular bulging of the prostatic contour (Fig 11), low signal intensity indicative of cancer in the rectoprostatic fat, and overt extracapsular cancer. The last three criteria have the highest sensitivity (96) while all criteria have high specificity.

There has been a longstanding debate on whether or not to use an endorectal coil for prostate cancer staging since its use results in a more labor-intensive and costly examination. In a meta-analysis, Engelbrecht et al (97) reported on 146 studies performed at 1.5 T and found that the use of turbo spin-echo sequences, an endorectal coil and multiplanar acquisitions all significantly increased staging performance. The application of an integrated endorectal-pelvic phased-array coil significantly improved staging performance, particularly sensitivity, compared with that of a pelvic phased-array coil alone: A_z increased from 0.57 to 0.74 at 1.5 T and from 0.62 to 0.68 at 3 T ($P < .001$) (98). Although, in the largest prospective prostate cancer staging study performed at 1.5 T of which we are aware (99), where MR imaging with a body coil only and with an endorectal coil only were compared, body coil imaging performed better (accuracy, 62%) than did endorectal coil imaging (accuracy, 52%). In the past decade since this trial, technologic developments such as the use as higher field strengths, improved pelvic phased-array coils and multiparametric MR imaging techniques have improved staging accuracy considerably. However, accuracy results vary between different studies. Table 2 provides an overview of recent prostate cancer staging MR imaging studies at both field strengths (100–107). The results of the MR prostate cancer staging studies, as presented in Table 2, seem conflicting. One should be careful, as difficulty remains in comparing and interpreting results of these studies because different field strengths, comparisons of coil types, and endpoints were used for prostate cancer staging.

To our knowledge, only two studies have directly compared 3-T and 1.5-T MR staging of prostate cancer (108,109). This comparison was suboptimal, because use of a pelvic phased-array coil at 3 T was compared with use of a pelvic phased-array coil and/or an endorectal coil at 1.5 T. Conclusions on the effects of higher field strength on MR staging of prostate cancer remain difficult to infer because research on this topic is still immature.

Multiparametric MR imaging may also improve prostate cancer staging. In a large prospective study with 99 patients (110), dynamic contrast-enhanced MR imaging combined with T2-weighted MR imaging significantly improved the accuracy of prostate cancer staging compared with that of T2-weighted MR imaging alone. A_z values for less

Figure 9

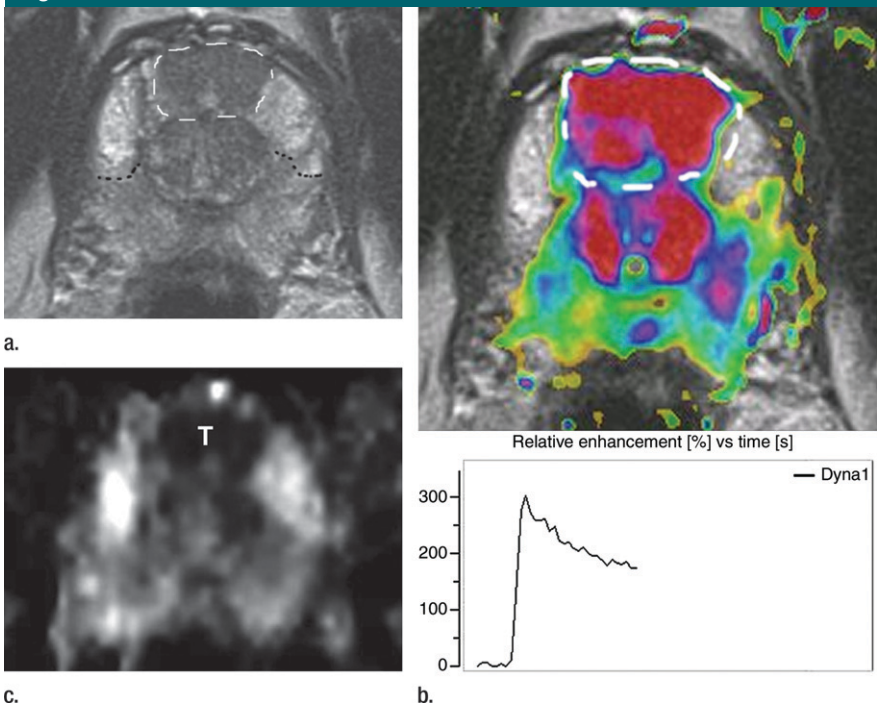

Figure 9: Added value of combined multiparametric MR imaging for prostate cancer detection in a 63-year-old man with PSA level of 27.5 ng/mL, clinical stage T0, and history of seven previous negative systematic random biopsy sessions (total of 96 cores). T2-weighted and dynamic contrast-enhanced MR imaging findings are indeterminate to suspicious for tumor within the transition zone, whereas ADC maps may help correct localization of this prostate cancer. **(a)** Axial T2-weighted turbo spin-echo MR image (4260/99; flip angle, 120°) at midprostate shows low-signal-intensity region in midventral prostate (white outline), which is suspicious for prostate cancer. Furthermore, peripheral zone from dorsal aspect to midline in dorsoventral plane has lower signal intensity than the anterior horns (black outline). This area did not show decreased ADC. This may be due to biopsy-related fibrosis. **(b)** Top: Same image as **a** with superimposed K^{trans} map (38/1.35; flip angle, 14°) shows high K^{trans} in midventral transition zone (outline), in addition to the mediodorsal transition zone. Bottom: Relative gadolinium concentration (y-axis) versus time (x-axis) curve *(Dyna1)* shows type 3 curve (fast increase and time to peak followed by washout). **(c)** Axial ADC map (2400/81; b = 0, 50, 500, and 800 sec/mm^2) at same level as **a** shows restriction (mean ADC = 750 × 10^{-6} mm^2/sec) in midventral transition zone *(T),* indicating intermediate to high tumor aggressiveness. MR-guided biopsy revealed a Gleason score 7 (3+4) prostate cancer.

experienced readers were 0.82 for dynamic contrast-enhanced plus T2-weighted MR imaging and 0.66 for T2-weighted imaging alone respectively ($P \leq .01$). In a prospective study with 53 patients (111), addition of three-dimensional MR spectroscopic imaging results to T2-weighted MR imaging results significantly improved accuracy for predicting extracapsular extension for both experienced and less-experienced readers (A_z increase from 0.78 to 0.86 and 0.62 to 0.75, respectively, for T2-weighted imaging only vs combined imaging).

Drawbacks of T2-weighted MR imaging for prostate cancer localization and local staging include differentiation of inflammatory changes from cancer. Furthermore, high inter- and intraobserver variability may lead to under- or overestimation of cancer stage (112). Also, postbiopsy hemorrhage can decrease staging accuracy. Finally, T2-weighted MR imaging cannot be used to detect microscopic capsular invasion. As mentioned earlier, pitfalls of multiparametric MR techniques also affect the ability to facilitate prostate cancer localization and local staging. (see Figs 5, 10).

Of all clinical indications for multiparametric MR imaging, localization is the most important. Accurate prostate cancer localization results in more accurate prostate cancer staging and in more accurate MR guidance of prostate biopsy and therapy.

Determination of Prostate Cancer Aggressiveness

Prostate cancer is graded according to the Gleason score, a combination of the two most prevalent Gleason grades (at prostatectomy) or the most prevalent and the highest grade (at prostate biopsy), based on architectural characteristics of prostate cancer tissue (113,114). Sampling error in biopsy specimens obtained at systematic random biopsy occurs in approximately in 64% of procedures (10) and results in a changed Gleason score at histopathologic evaluation of the prostatectomy specimen. This results in incorrect evaluation of prostate cancer aggressiveness, which may cause under- or overtreatment (115).

On T2-weighted MR images, signal intensity changes and detection rates for prostate cancer have been associated with its aggressiveness. In a retrospective study with 74 patients, in which prostatectomy specimens were used as standard of reference (14), low-grade cancers were detected at a rate of 43%, while high-grade cancers were detected at a rate of 79%. In another retrospective study, which also used prostatectomy specimens as reference standard (116), higher Gleason scores were associated with lower tumor-to-muscle signal intensity ratios on T2-weighted MR images. In a large retrospective study with 220 patients (117), T2-weighted MR imaging and MR spectroscopic imaging scores based on a three-point scale for clinical prostate cancer aggressiveness were significantly correlated to biologic markers such as androgen receptor levels, which were associated with prostate cancer progression. In that study, the combination of biologic markers with T2-weighted MR imaging and MR spectroscopic imaging results yielded an A_z of 0.91 for discrimination of clinically unimportant prostate cancer, which was defined as

Figure 10

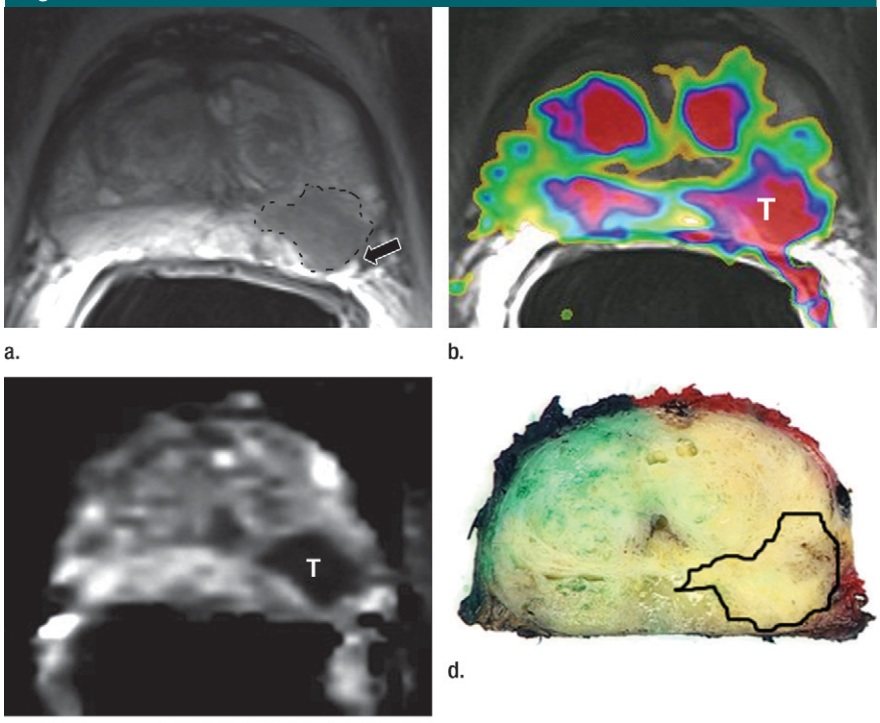

Figure 10: Multiparametric MR imaging for prostate cancer localization in a 71-year-old man with stage T1, Gleason score of 7 (3+4) disease in left prostate base who underwent endorectal MR staging: pitfalls in dynamic contrast-enhanced MR imaging localization of prostate cancer. Dynamic contrast-enhanced MR imaging results in enhancement in multiple areas and is therefore indeterminate when performed in addition to T2-weighted MR imaging. DW imaging correctly localizes this cancer and shows its aggressiveness. **(a)** Axial T2-weighted turbo spin-echo MR image (4260/99; flip angle, 120°) at midprostate shows low-signal-intensity lesion in left peripheral zone (outline) next to region of high signal intensity in peripheral zone, with minimal signs of extracapsular extension (arrow). **(b)** Axial MR image with a superimposed K^{trans} map (38/1.35; flip angle, 14°) at same level as **a** shows multiple enhancing areas in both peripheral and transition zones. Tumor area *(T)* also shows enhancement. Tumor localization is indeterminate. **(c)** Axial ADC map (2400/81; b = 0, 50, 500, and 800 sec/mm^2) at same level as **a** shows restricted diffusion in laterodorsal peripheral zone *(T)* (mean ADC = 808 × 10^{-6} mm^2/sec), which indicates intermediate tumor aggressiveness. **(d)** Axial whole-mount histopathologic slice at level corresponding to that of **a–c** shows a Gleason score 7 (3+4), stage T3A prostate cancer in the left laterodorsal peripheral zone (outline), which confirms the T2-weighted and DW imaging data.

Figure 11

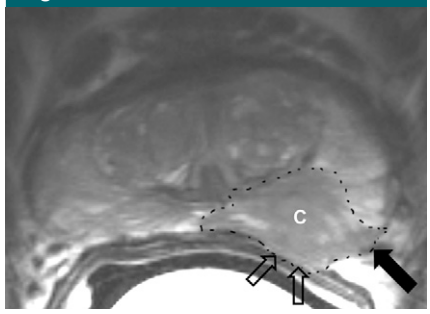

Figure 11: Multiparametric MR imaging in prostate cancer staging in a 70-year-old man with PSA level of 12 ng/mL and well-differentiated prostate carcinoma *(C)*. Axial T2-weighted turbo spin-echo MR image (4260/99; flip angle, 120°) shows low-signal-intensity region (outline) in left peripheral zone. Bulging and obliteration of rectoprostatic angle (open arrows) indicate extracapsular extension. There is invasion of the neurovascular bundle (solid arrow). At MR imaging, stage T3a prostate cancer was reported. Radical prostatectomy revealed a solitary adenocarcinoma with Gleason score 7 (3+4) with extraprostatic extension (stage T3a).

cancer confined to the organ and 0.5 cm^3 or less in volume without poorly differentiated parts at pathologic examination.

Moreover, at MR spectroscopic imaging, the choline-plus-creatine–to-citrate ratios have been shown to be associated with Gleason score (118,119). In a retrospective study of 43 patients with biopsy-proved prostate cancer, Kobus et al (120) showed that 3-T MR spectroscopic imaging is an accurate technique for discriminating patients with Gleason grade 2 or 3 cancer from patients with Gleason score 4 or 5 cancer, as determined with prostatectomy specimens. By using a standardized-threshold approach involving both the choline-plus-creatine–to-citrate ratio and the choline-to-citrate ratio, an A_z of 0.78 was achieved for discrimination of Gleason score 2–3 from Gleason score 4–5 prostate cancers.

Results for ADC as a possible marker of cancer aggressiveness are very promising: In a retrospective study of 3-T DW imaging (b = 0, 50, 500, and 800 sec/mm^2) Hambrock et al (45) correlated median ADCs with prostatectomy Gleason grades in peripheral zone prostate cancers on a slice-by-slice basis in 51 patients. Cancers with Gleason score 2–3 components were discerned from cancers with Gleason score 4–5 components, with an A_z of 0.90. Furthermore, in a study of 1.5-T DW imaging (b = 0 and 600 sec/mm^2) in 110 patients with 197 tumors, Verma and Rajesh (121) found a negative correlation (r = −0.39) between mean ADC and Gleason score for peripheral zone cancers on prostatectomy specimens. A similar association could not be found for cancers in the transition zone. An A_z of 0.78 was achieved by using both cancer volume and ADC as predictors of tumor aggressiveness (Gleason score > 6). While preliminary studies in the field of prostate cancer aggressiveness show promising results (45), different parameters from different multiparametric techniques show some overlap among Gleason scores. Because a certain value of an MR parameter, such as ADC, cannot be precisely associated with one Gleason score component, multiparametric MR imaging cannot yet be applied to the determination of prostate cancer aggressiveness in a general

Table 2

Diagnostic Statistics for MR Studies of Prostate Cancer Staging Since 2006

Study and Year	Field Strength (T)	No. of Subjects	PA Coil	ER Coil	MR Technique	Sensitivity (%)*	Specificity (%)*	Accuracy (%)*
Lee et al (107), 2010	1.5	91	Yes	Yes	T2 weighted, DW	PA: ECE in 30 (8/27), SVI in 50 (2/4); ER: ECE in 32 (7/22), SVI in 50 (2/4)	PA: ECE in 90 (18/20), SVI in 98 (42/43); ER: ECE in 96 (21/22), SVI in 93 (37/40)	NR
Augustin et al (100), 2009	3.0	27	Yes	No	T2 weighted	ECE in 67 (4/6)	ECE in 100 (21/21)	ECE in 85 (23/27)
Porcaro et al (103), 2009	1.5	154	NR	Yes	T2 weighted	ECE in 78; SVI in 88	ECE in 96; SVI in 98	ECE in 91; SVI in 97
Torricelli et al (104), 2008	3.0	42	Yes	No	T2 and T1 weighted	ECE in 69 (11/16)†	ECE in 92 (24/26)†	ECE in 83 (35/42)†
Park et al (109), 2007	3.0	54	Yes	No	T2 weighted	ECE in 81 (17/21); SVI in 50 (1/2)	ECE in 67 (22/33); SVI in 100 (52/52)	ECE in 72 (39/54); SVI in 98 (53/54)
Park et al (109), 2007	1.5	54	No	Yes	T2 weighted	ECE in 71 (10/14); SVI in 75 (3/4)	ECE in 73 (29/40); SVI in 92 (46/50)	ECE in 72 (39/54); SVI in 91 (49/54)
Heijmink et al (102), 2007	3.0	46	Yes	Yes	T2 weighted	PA: 13 (2/15); ERC: 80 (12/15)‡	PA: 100 (31/31); ERC: 100 (31/31)‡	PA: 70 (32/46); ERC: 93 (43/46)‡
Futterer et al (98), 2007	1.5	81	Yes	Yes	T2 weighted	64 (23/36)	98 (44/45)	83 (67/82)
Bloch et al (106), 2007	1.5	32	Yes	Yes	T2 weighted, dynamic contrast enhanced	ECE in 91 (11/12)§	ECE in 95 (21/22)§	NR
Chandra et al (101), 2007	1.5	38	Yes	Yes	T2 weighted, MR spectroscopic imaging	ECE in 69; SVI in 60	ECE in 82 SVI in 100	ECE in 76 SVI in 95
Latcham-setty et al (105), 2007	1.5	80	NR	Yes	T2 weighted	ECE in 71‖	ECE in 78‖	ECE in 73‖
Futterer et al (96), 2006	3.0	32	Yes	Yes	T2 and T1 weighted	88 (7/8)	96 (23/24)	94 (30/32)

Note.—Reference standard in all studies was prostatectomy specimen. ECE = extracapsular extension, ER = endorectal, NR = not reported, PA = pelvic phased array, SVI = seminal vesicle invasion.

*Data in parentheses are numbers from which percentages were calculated.

†Obtained by experienced radiologist.

‡Maximal values for an examination performed independently by four radiologists.

§Maximal percentages for assessment of extracapsular extension adjusted to prevalence of disease in the study population at large.

‖Highest values from two separate groups of 40 patients.

clinical environment. However, this technique is very helpful for assessing tumor grade and guiding biopsy to the most aggressive part of the tumor.

Active Surveillance

With the observation that low-risk cancers do not progress rapidly when treatment is deferred (122,123), implementation of active surveillance protocols has become more widespread. The aim of this approach is to minimize overtreatment by mean of active observation of low-risk cancers and to intervene with curative therapy when a presumably low-risk cancer shows signs of progression. Low-risk cancer is frequently defined as a cancer with a clinical stage of T2 or lower, a Gleason score of 6 or less without a Gleason 4 or 5 component, a PSA level of 10 ng/mL or less, a PSA density ≤0.15 ng/mL/mL or less, and systematic random biopsy criteria of two or fewer cores with prostate cancer and 50% volume of cancer or less per core (124).

The cornerstone of active surveillance protocols is the accurate identification of low-risk cancers. A frequent cause for inaccurate estimation of prostate cancer aggressiveness is sampling error at systematic random biopsy with subsequent undergrading of Gleason score. In addition, cancer volume is also often underestimated owing to sampling error in systematic random biopsies, because cancer volume is estimated by measuring the number and volume percentages of cancer tissue of cancer-positive biopsy cores (10). In patients in whom risk stratification was incorrectly determined, repeat biopsies may eventually show evidence of high-risk disease, which then triggers a delayed intervention with, perhaps, a missed opportunity for definitive curative therapy (125–127).

Multiparametric MR imaging can potentially aid in adequate risk stratification for patient selection in active surveillance by improving prostate cancer staging and by characterizing cancer aggressiveness (Fig 6). An example of improved staging by using MR imaging

in active surveillance is in a prospective study by Berglund et al (128). In that study, 18 (39%) of 66 patients in whom MR imaging findings were suspicious for extracapsular extension were upgraded or upstaged because of progression at histologic examination of the repeat biopsy specimen.

During follow-up in active surveillance, detection of cancer progression within the curative window is essential. MR imaging can also be valuable in this application. Recently, Giles et al (129) showed that ADCs at repeat biopsy were significantly lower in patients with a Gleason score increase than in those with a stable score ($P < .001$). In that study, both tumor volume ($P = .002$) and ADCs calculated from DW imaging (300–800 sec/mm^2) ($P = .02$) were significant independent predictors of progression of active surveillance patients. Progression was defined biochemically (PSA increase, >1 ng/mL per year) and/or histopathologically (repeat biopsy Gleason grade > 4 or cancer presence in more than 50% of biopsy cores). In another active surveillance study in 86 patients with a mean follow-up of 29 months (130), DW imaging tumor ADC data were significant predictors of a Gleason score 4 component at repeat biopsy ($A_z = 0.70$, $P < .001$) and of the need for initiation of radical treatment during follow-up ($A_z = 0.83$, $P < .001$). Patients were included in this study if they met the following criteria: PSA level of 15 ng/mL or lower, Gleason score of 7 or lower with a primary Gleason score of 3 or less, 50% or fewer of biopsy cores positive at systematic random biopsy, three monthly PSA measurements, repeat systematic random biopsies 12–24 months after inclusion, and performance of DWI imaging before inclusion. Similar results were found in another retrospective study (131), in which an increase to Gleason score 7 or higher at subsequent repeat systematic random biopsy in 114 active surveillance patients was associated with T2-weighted MR imaging results although not with transrectal US or MR spectroscopic imaging results.

These studies may underestimate results because systematic random biopsy specimens, instead of a prostatectomy specimen, were used as the reference standard. On the other hand, in a large retrospective study, Cabrera et al (132) found that T2-weighted MR imaging and MR spectroscopic imaging performed at baseline were of no additional prognostic value to active surveillance because the presence of cancer on MR images could not be associated with biochemical outcome in multivariate analysis. Biochemical outcome was defined according to serial PSA measurements, which were classified as stable or progressive by using slopes of regression lines. These results conflict with those of previous retrospective studies (130,131). The field strength of 1.5 T used by Cabrera et al and the use of PSA kinetics instead of histologic findings as a measure of prostate cancer progression might partly explain these conflicting results. Despite general promising results, incorporation of multiparametric MR imaging into active surveillance protocols for low-risk prostate cancer is still in an early phase.

Multiparametric MR imaging and MR-guided biopsy may improve initial diagnosis and accurate monitoring of prostate cancer stage and aggressiveness in active surveillance. Future research addressing the use of multiparametric MR imaging in selection and follow-up of patients with low-risk prostate cancer as part of active surveillance protocols is needed.

Conclusion

In this review, we have presented and discussed available data on the additional value of the different functional MR imaging techniques in various clinical diagnostic prostate cancer problems.

To increase MR imaging accuracy for the different clinical prostate cancer indications, one or more functional MR imaging techniques should be combined with T2-weighted MR imaging in a multiparametric MR examination of the prostate. However, within the variety of different acquisition methods, protocols, magnetic field strengths and multiparametric techniques that are used, consensus guidelines on dedicated MR protocols for specific clinical indications are lacking.

Suggested minimal requirements for a multiparametric MR imaging protocol for clinical evaluation of prostate cancer are T1- and T2-weighted MR imaging in combination with DW and dynamic contrast-enhanced MR imaging. T1-and T2-weighted MR imaging should be used for evaluation of anatomy. Dynamic contrast-enhanced MR imaging can be used for high-sensitivity identification of potential prostate cancer locations. Unfortunately, little standardization in dynamic contrast-enhanced MR acquisition and analysis exists. DW imaging or MR spectroscopic imaging are accurate functional MR techniques, and they may be added to improve specificity for different clinical indications. DW imaging is the most practical and simple accurate functional imaging technique; however, it is prone to motion and susceptibility artifacts. MR spectroscopic imaging is an accurate technique that, like DW imaging, can be used for assessing prostate cancer aggressiveness. Expertise and longer imaging times are prerequisites for MR spectroscopic imaging, which may ultimately decrease its clinical applicability.

Because the reported accuracies of multiparametric MR imaging techniques for different indications are inconsistent, definitive conclusions on the accuracies of (combined) multiparametric MR imaging techniques for a particular clinical prostate cancer problem are difficult to make. In general, the addition of functional MR techniques to T2-weighted MR imaging improves accuracy for both localization and local staging of prostate cancer in comparison to the accuracy of T2-weighted MR imaging alone. Of all clinical indications for multiparametric MR imaging of the prostate, localization is the most important. Accurate determination of prostate cancer location(s) results in more accurate prostate cancer staging and MR guidance of prostate biopsy and therapy.

Currently, multiparametric MR imaging is performed at only a limited number of centers worldwide. Development of expertise in functional MR

techniques and increased availability of equipment are needed, so that multiparametric prostate MR imaging can become a more accessible examination. To warrant accurate future multiparametric MR imaging prostate cancer diagnostics, computer programs are needed to support clinicians by allowing simple postprocessing and fast evaluation of the data.

Acknowledgment: The authors thank Yvonne Hoogeveen, PhD, for editing the manuscript.

HH, IMvO, JAW, AH, JJF

Disclosures of Potential Conflicts of Interest: C.A.H. No potential conflicts of interest to disclose. **J.O.B.** No potential conflicts of interest to disclose. **T.H.** No potential conflicts of interest to disclose. **D.Y.** No potential conflicts of interest to disclose. **D.M.S.** No potential conflicts of interest to disclose. **S.W.T.P.J.H.** No potential conflicts of interest to disclose. **T.W.J.S.** Financial activities related to the present article: none to disclose. Financial activity not related to the present article: received a grant or has grants pending from Siemens Healthcare. Other relationships: none to disclose. **P.C.V.** No potential conflicts of interest to disclose. **H.H.** No potential conflicts of interest to disclose. **I.M.v.O.** No potential conflicts of interest to disclose. **J.A.W.** No potential conflicts of interest to disclose. **A.H.** Financial activities related to the present article: Institution has received funds for consultancy for Siemens Healthcare. Other relationships: none to disclose. **J.J.F.** Financial activities related to the present article: Received a grant or has grants pending from Siemens Healthcare. Financial activities not related to the present article: none to disclose. Other relationships: none to disclose.

References

1. Parkin DM, Bray F, Ferlay J, Pisani P. Global cancer statistics, 2002. CA Cancer J Clin 2005;55(2):74–108.
2. Gleason DF. Histologic grading of prostate cancer: a perspective. Hum Pathol 1992; 23(3):273–279.
3. Egevad L, Granfors T, Karlberg L, Bergh A, Stattin P. Prognostic value of the Gleason score in prostate cancer. BJU Int 2002; 89(6):538–542.
4. Partin AW, Mangold LA, Lamm DM, Walsh PC, Epstein JI, Pearson JD. Contemporary update of prostate cancer staging nomograms (Partin Tables) for the new millennium. Urology 2001;58(6):843–848.
5. Schröder FH, van der Maas P, Beemsterboer P, et al. Evaluation of the digital rectal examination as a screening test for prostate cancer. Rotterdam section of the European Randomized Study of Screening for Prostate Cancer. J Natl Cancer Inst 1998;90(23):1817–1823.
6. Catalona WJ, Richie JP, Ahmann FR, et al. Comparison of digital rectal examination and serum prostate specific antigen in the early detection of prostate cancer: results of a multicenter clinical trial of 6,630 men. J Urol 1994;151(5):1283–1290.
7. Schröder FH, Carter HB, Wolters T, et al. Early detection of prostate cancer in 2007. Part 1: PSA and PSA kinetics. Eur Urol 2008;53(3):468–477.
8. Donovan J, Hamdy F, Neal D, et al. Prostate Testing for Cancer and Treatment (ProtecT) feasibility study. Health Technol Assess 2003;7(14):1–88.
9. Djavan B, Ravery V, Zlotta A, et al. Prospective evaluation of prostate cancer detected on biopsies 1, 2, 3 and 4: when should we stop? J Urol 2001;166(5):1679–1683.
10. Noguchi M, Stamey TA, McNeal JE, Yemoto CM. Relationship between systematic biopsies and histological features of 222 radical prostatectomy specimens: lack of prediction of tumor significance for men with nonpalpable prostate cancer. J Urol 2001;166(1):104–109; discussion 109–110.
11. Steyn JH, Smith FW. Nuclear magnetic resonance imaging of the prostate. Br J Urol 1982;54(6):726–728.
12. Hricak H, Williams RD, Spring DB, et al. Anatomy and pathology of the male pelvis by magnetic resonance imaging. AJR Am J Roentgenol 1983;141(6):1101–1110.
13. Hricak H, Dooms GC, McNeal JE, et al. MR imaging of the prostate gland: normal anatomy. AJR Am J Roentgenol 1987; 148(1):51–58.
14. Wang L, Mazaheri Y, Zhang J, Ishill NM, Kuroiwa K, Hricak H. Assessment of biologic aggressiveness of prostate cancer: correlation of MR signal intensity with Gleason grade after radical prostatectomy. Radiology 2008;246(1):168–176.
15. Langer DL, van der Kwast TH, Evans AJ, et al. Intermixed normal tissue within prostate cancer: effect on MR imaging measurements of apparent diffusion coefficient and T2—sparse versus dense cancers. Radiology 2008;249(3):900–908.
16. Kirkham AP, Emberton M, Allen C. How good is MRI at detecting and characterising cancer within the prostate? Eur Urol 2006;50(6):1163–1174; discussion 1175.
17. Cruz M, Tsuda K, Narumi Y, et al. Characterization of low-intensity lesions in the peripheral zone of prostate on pre-biopsy endorectal coil MR imaging. Eur Radiol 2002;12(2):357–365.
18. Qayyum A, Coakley FV, Lu Y, et al. Organ-confined prostate cancer: effect of prior transrectal biopsy on endorectal MRI and MR spectroscopic imaging. AJR Am J Roentgenol 2004;183(4):1079–1083.
19. Akin O, Sala E, Moskowitz CS, et al. Transition zone prostate cancers: features, detection, localization, and staging at endorectal MR imaging. Radiology 2006;239(3): 784–792.
20. Bonekamp D, Macura KJ. Dynamic contrast-enhanced magnetic resonance imaging in the evaluation of the prostate. Top Magn Reson Imaging 2008;19(6):273–284.
21. Huisman HJ, Engelbrecht MR, Barentsz JO. Accurate estimation of pharmacokinetic contrast-enhanced dynamic MRI parameters of the prostate. J Magn Reson Imaging 2001;13(4):607–614.
22. Alonzi R, Padhani AR, Allen C. Dynamic contrast enhanced MRI in prostate cancer. Eur J Radiol 2007;63(3):335–350.
23. Barentsz JO, Engelbrecht M, Jager GJ, et al. Fast dynamic gadolinium-enhanced MR imaging of urinary bladder and prostate cancer. J Magn Reson Imaging 1999; 10(3):295–304.
24. Engelbrecht MR, Huisman HJ, Laheij RJ, et al. Discrimination of prostate cancer from normal peripheral zone and central gland tissue by using dynamic contrast-enhanced MR imaging. Radiology 2003; 229(1):248–254.
25. Padhani AR, Harvey CJ, Cosgrove DO. Angiogenesis imaging in the management of prostate cancer. Nat Clin Pract Urol 2005;2(12):596–607.
26. Weinmann HJ, Laniado M, Mützel W. Pharmacokinetics of GdDTPA/dimeglumine after intravenous injection into healthy volunteers. Physiol Chem Phys Med NMR 1984;16(2):167–172.
27. Kovar DA, Lewis M, Karczmar GS. A new method for imaging perfusion and contrast extraction fraction: input functions derived from reference tissues. J Magn Reson Imaging 1998;8(5):1126–1134.
28. Kety SS. The theory and applications of the exchange of inert gas at the lungs and tissues. Pharmacol Rev 1951;3(1):1–41.
29. Tofts PS. Modeling tracer kinetics in dynamic Gd-DTPA MR imaging. J Magn Reson Imaging 1997;7(1):91–101.
30. Larsson HB, Fritz-Hansen T, Rostrup E, Søndergaard L, Ring P, Henriksen O. Myocardial perfusion modeling using MRI. Magn Reson Med 1996;35(5):716–726.

31. St Lawrence KS, Lee TY. An adiabatic approximation to the tissue homogeneity model for water exchange in the brain: I. Theoretical derivation. J Cereb Blood Flow Metab 1998;18(12):1365–1377.

32. Tofts PS, Brix G, Buckley DL, et al. Estimating kinetic parameters from dynamic contrast-enhanced T(1)-weighted MRI of a diffusable tracer: standardized quantities and symbols. J Magn Reson Imaging 1999;10(3):223–232.

33. Franiel T, Lüdemann L, Rudolph B, et al. Evaluation of normal prostate tissue, chronic prostatitis, and prostate cancer by quantitative perfusion analysis using a dynamic contrast-enhanced inversion-prepared dual-contrast gradient echo sequence. Invest Radiol 2008;43(7):481–487.

34. Jager GJ, Ruijter ET, van de Kaa CA, et al. Local staging of prostate cancer with endorectal MR imaging: correlation with histopathology. AJR Am J Roentgenol 1996; 166(4):845–852.

35. Schlemmer HP, Merkle J, Grobholz R, et al. Can pre-operative contrast-enhanced dynamic MR imaging for prostate cancer predict microvessel density in prostatectomy specimens? Eur Radiol 2004;14(2):309–317.

36. Stejskal EO, Tanner JE. Spin diffusion measurements: spin echoes in the presence of a time-dependent field gradient. J Chem Phys 1965;42(1):288–292.

37. Jacobs MA, Ouwerkerk R, Petrowski K, Macura KJ. Diffusion-weighted imaging with apparent diffusion coefficient mapping and spectroscopy in prostate cancer. Top Magn Reson Imaging 2008;19(6):261–272.

38. Somford DM, Fütterer JJ, Hambrock T, Barentsz JO. Diffusion and perfusion MR imaging of the prostate. Magn Reson Imaging Clin N Am 2008;16(4):685–695, ix.

39. Kim CK, Park BK, Kim B. High-b-value diffusion-weighted imaging at 3 T to detect prostate cancer: comparisons between b values of 1,000 and 2,000 s/mm2. AJR Am J Roentgenol 2010;194(1):W33–W37.

40. Katahira K, Takahara T, Kwee TC, et al. Ultra-high-b-value diffusion-weighted MR imaging for the detection of prostate cancer: evaluation in 201 cases with histopathological correlation. Eur Radiol 2011; 21(1):188–196.

41. Gibbs P, Tozer DJ, Liney GP, Turnbull LW. Comparison of quantitative T2 mapping and diffusion-weighted imaging in the normal and pathologic prostate. Magn Reson Med 2001;46(6):1054–1058.

42. Zelhof B, Pickles M, Liney G, et al. Correlation of diffusion-weighted magnetic resonance data with cellularity in prostate cancer. BJU Int 2009;103(7):883–888.

43. Hosseinzadeh K, Schwarz SD. Endorectal diffusion-weighted imaging in prostate cancer to differentiate malignant and benign peripheral zone tissue. J Magn Reson Imaging 2004;20(4):654–661.

44. Kim JH, Kim JK, Park BW, Kim N, Cho KS. Apparent diffusion coefficient: prostate cancer versus noncancerous tissue according to anatomical region. J Magn Reson Imaging 2008;28(5):1173–1179.

45. Hambrock T, Somford DM, Huisman HJ, et al. Relationship between apparent diffusion coefficients at 3.0-T MR imaging and Gleason grade in peripheral zone prostate cancer. Radiology 2011;259(2):453–461.

46. Bammer R. Basic principles of diffusion-weighted imaging. Eur J Radiol 2003; 45(3):169–184.

47. Heerschap A, Jager GJ, van der Graaf M, Barentsz JO, Ruijs SH. Proton MR spectroscopy of the normal human prostate with an endorectal coil and a double spin-echo pulse sequence. Magn Reson Med 1997;37(2):204–213.

48. Kurhanewicz J, Vigneron DB, Nelson SJ, et al. Citrate as an in vivo marker to discriminate prostate cancer from benign prostatic hyperplasia and normal prostate peripheral zone: detection via localized proton spectroscopy. Urology 1995;45(3): 459–466.

49. Heerschap A, Jager GJ, van der Graaf M, et al. In vivo proton MR spectroscopy reveals altered metabolite content in malignant prostate tissue. Anticancer Res 1997; 17(3A):1455–1460.

50. Cornel EB, Smits GA, Oosterhof GO, et al. Characterization of human prostate cancer, benign prostatic hyperplasia and normal prostate by in vitro 1H and 31P magnetic resonance spectroscopy. J Urol 1993; 150(6):2019–2024.

51. Mueller-Lisse UG, Scherr MK. Proton MR spectroscopy of the prostate. Eur J Radiol 2007;63(3):351–360.

52. Mescher M, Tannus A, O'Neil Johnson M, Garwood M. Solvent suppression using selective echo dephasing. J Magn Reson A 1996;123(2):226–229.

53. Star-Lack J, Nelson SJ, Kurhanewicz J, Huang LR, Vigneron DB. Improved water and lipid suppression for 3D PRESS CSI using RF band selective inversion with gradient dephasing (BASING). Magn Reson Med 1997;38(2):311–321.

54. Scheenen TW, Klomp DW, Röll SA, Fütterer JJ, Barentsz JO, Heerschap A. Fast acquisition-weighted three-dimensional proton MR spectroscopic imaging of the human prostate. Magn Reson Med 2004; 52(1):80–88.

55. Scheenen TW, Gambarota G, Weiland E, et al. Optimal timing for in vivo 1H-MR spectroscopic imaging of the human prostate at 3T. Magn Reson Med 2005;53(6): 1268–1274.

56. Dickinson L, Ahmed HU, Allen C, et al. Magnetic resonance imaging for the detection, localisation, and characterisation of prostate cancer: recommendations from a European consensus meeting. Eur Urol 2011;59(4):477–494.

57. Hambrock T, Somford DM, Hoeks C, et al. Magnetic resonance imaging guided prostate biopsy in men with repeat negative biopsies and increased prostate specific antigen. J Urol 2010;183(2):520–527.

58. Vos PC. Combining T2-weighted with dynamic MR images for computerized classification of prostate lesions. In: Editor A, Editor B, eds. Proceedings of SPIE: medical imaging 2008—title. Vol 6915. Bellingham, Wash: SPIE–The International Society for Optical Engineering, 2008.

59. Puech P, Betrouni N, Makni N, Dewalle AS, Villers A, Lemaitre L. Computer-assisted diagnosis of prostate cancer using DCE-MRI data: design, implementation and preliminary results. Int J CARS 2009;4(1):1–10.

60. Vos PC, Hambrock T, Hulsbergen-van de Kaa CA, Fütterer JJ, Barentsz JO, Huisman HJ. Computerized analysis of prostate lesions in the peripheral zone using dynamic contrast enhanced MRI. Med Phys 2008;35(3):888–899.

61. Ruprecht O, Weisser P, Bodelle B, Ackermann H, Vogl TJ. MRI of the prostate: Interobserver agreement compared with histopathologic outcome after radical prostatectomy. Eur J Radiol 2011 Feb 26. [Epub ahead of print]

62. Beyersdorff D, Winkel A, Hamm B, Lenk S, Loening SA, Taupitz M. MR imaging-guided prostate biopsy with a closed MR unit at 1.5 T: initial results. Radiology 2005;234(2):576–581.

63. Engelhard K, Hollenbach HP, Kiefer B, Winkel A, Goeb K, Engehausen D. Prostate biopsy in the supine position in a standard 1.5-T scanner under real time MR-imaging control using a MR-compatible endorectal biopsy device. Eur Radiol 2006;16(6):1237–1243.

64. Roethke M, Anastasiadis AG, Lichy M, et al. MRI-guided prostate biopsy detects clinically significant cancer: analysis of a

cohort of 100 patients after previous negative TRUS biopsy. World J Urol 2011 Apr 22. [Epub ahead of print]

65. Roehl KA, Antenor JA, Catalona WJ. Serial biopsy results in prostate cancer screening study. J Urol 2002;167(6):2435–2439.

66. Franiel T, Stephan C, Erbersdobler A, et al. Areas suspicious for prostate cancer: MR-guided biopsy in patients with at least one transrectal US-guided biopsy with a negative finding—multiparametric MR imaging for detection and biopsy planning. Radiology 2011;259(1):162–172.

67. Pondman KM, Fütterer JJ, ten Haken B, et al. MR-guided biopsy of the prostate: an overview of techniques and a systematic review. Eur Urol 2008;54(3):517–527.

68. Kumar V, Jagannathan NR, Kumar R, et al. Transrectal ultrasound-guided biopsy of prostate voxels identified as suspicious of malignancy on three-dimensional (1)H MR spectroscopic imaging in patients with abnormal digital rectal examination or raised prostate specific antigen level of 4-10 ng/ml. NMR Biomed 2007;20(1):11–20.

69. Prando A, Kurhanewicz J, Borges AP, Oliveira EM Jr, Figueiredo E. Prostatic biopsy directed with endorectal MR spectroscopic imaging findings in patients with elevated prostate specific antigen levels and prior negative biopsy findings: early experience. Radiology 2005;236(3):903–910.

70. Labanaris AP, Zugor V, Smiszek R, Nützel R, Kühn R, Engelhard K. Guided e-MRI prostate biopsy can solve the discordance between Gleason score biopsy and radical prostatectomy pathology. Magn Reson Imaging 2010;28(7):943–946.

71. Kaplan I, Oldenburg NE, Meskell P, Blake M, Church P, Holupka EJ. Real time MRI-ultrasound image guided stereotactic prostate biopsy. Magn Reson Imaging 2002;20(3):295–299.

72. Singh AK, Kruecker J, Xu S, et al. Initial clinical experience with real-time transrectal ultrasonography-magnetic resonance imaging fusion-guided prostate biopsy. BJU Int 2008;101(7):841–845.

73. Langer DL, van der Kwast TH, Evans AJ, Trachtenberg J, Wilson BC, Haider MA. Prostate cancer detection with multi-parametric MRI: logistic regression analysis of quantitative T2, diffusion-weighted imaging, and dynamic contrast-enhanced MRI. J Magn Reson Imaging 2009;30(2):327–334.

74. Puech P, Potiron E, Lemaitre L, et al. Dynamic contrast-enhanced-magnetic resonance imaging evaluation of intraprostatic prostate cancer: correlation with radical prostatectomy specimens. Urology 2009;74(5):1094–1099.

75. Langer DL, van der Kwast TH, Evans AJ, et al. Prostate tissue composition and MR measurements: investigating the relationships between ADC, T2, K(trans), v(e), and corresponding histologic features. Radiology 2010;255(2):485–494.

76. Delongchamps NB, Rouanne M, Flam T, et al. Multiparametric magnetic resonance imaging for the detection and localization of prostate cancer: combination of T2-weighted, dynamic contrast-enhanced and diffusion-weighted imaging. BJU Int 2011;107(9):1411–1418.

77. Villeirs GM, Oosterlinck W, Vanherreweghe E, De Meerleer GO. A qualitative approach to combined magnetic resonance imaging and spectroscopy in the diagnosis of prostate cancer. Eur J Radiol 2010;73(2):352–356.

78. Casciani E, Polettini E, Bertini L, et al. Contribution of the MR spectroscopic imaging in the diagnosis of prostate cancer in the peripheral zone. Abdom Imaging 2007 Feb 10. [Epub ahead of print]

79. Yoshizako T, Wada A, Hayashi T, et al. Usefulness of diffusion-weighted imaging and dynamic contrast-enhanced magnetic resonance imaging in the diagnosis of prostate transition-zone cancer. Acta Radiol 2008;49(10):1207–1213.

80. Mullerad M, Hricak H, Kuroiwa K, et al. Comparison of endorectal magnetic resonance imaging, guided prostate biopsy and digital rectal examination in the preoperative anatomical localization of prostate cancer. J Urol 2005;174(6):2158–2163.

81. Hricak H, White S, Vigneron D, et al. Carcinoma of the prostate gland: MR imaging with pelvic phased-array coils versus integrated endorectal—pelvic phased-array coils. Radiology 1994;193(3):703–709.

82. Scheidler J, Hricak H, Vigneron DB, et al. Prostate cancer: localization with three-dimensional proton MR spectroscopic imaging—clinicopathologic study. Radiology 1999;213(2):473–480.

83. Haider MA, van der Kwast TH, Tanguay J, et al. Combined T2-weighted and diffusion-weighted MRI for localization of prostate cancer. AJR Am J Roentgenol 2007;189(2):323–328.

84. Turkbey B, Pinto PA, Mani H, et al. Prostate cancer: value of multiparametric MR imaging at 3 T for detection—histopathologic correlation. Radiology 2010;255(1):89–99.

85. Fütterer JJ, Heijmink SW, Scheenen TW, et al. Prostate cancer localization with dynamic contrast-enhanced MR imaging and proton MR spectroscopic imaging. Radiology 2006;241(2):449–458.

86. Ogura K, Maekawa S, Okubo K, et al. Dynamic endorectal magnetic resonance imaging for local staging and detection of neurovascular bundle involvement of prostate cancer: correlation with histopathologic results. Urology 2001;57(4):721–726.

87. Jager GJ, Ruijter ET, van de Kaa CA, et al. Dynamic TurboFLASH subtraction technique for contrast-enhanced MR imaging of the prostate: correlation with histopathologic results. Radiology 1997;203(3):645–652.

88. Kim CK, Park BK, Kim B. Localization of prostate cancer using 3T MRI: comparison of T2-weighted and dynamic contrast-enhanced imaging. J Comput Assist Tomogr 2006;30(1):7–11.

89. Kim CK, Park BK, Lee HM, Kwon GY. Value of diffusion-weighted imaging for the prediction of prostate cancer location at 3T using a phased-array coil: preliminary results. Invest Radiol 2007;42(12):842–847.

90. Lim HK, Kim JK, Kim KA, Cho KS. Prostate cancer: apparent diffusion coefficient map with T2-weighted images for detection—a multireader study. Radiology 2009;250(1):145–151.

91. Vargas HA, Akin O, Franiel T, et al. Diffusion-weighted endorectal MR imaging at 3 T for prostate cancer: tumor detection and assessment of aggressiveness. Radiology 2011;259(3):775–784.

92. Wefer AE, Hricak H, Vigneron DB, et al. Sextant localization of prostate cancer: comparison of sextant biopsy, magnetic resonance imaging and magnetic resonance spectroscopic imaging with step section histology. J Urol 2000;164(2):400–404.

93. Weinreb JC, Blume JD, Coakley FV, et al. Prostate cancer: sextant localization at MR imaging and MR spectroscopic imaging before prostatectomy—results of ACRIN prospective multi-institutional clinicopathologic study. Radiology 2009;251(1):122–133.

94. Hoedemaeker RF, Vis AN, Van Der Kwast TH. Staging prostate cancer. Microsc Res Tech 2000;51(5):423–429.

95. Bostwick DG. Staging prostate cancer—1997: current methods and limitations. Eur Urol 1997;32(Suppl 3):2–14.

96. Fütterer JJ, Heijmink SW, Scheenen TW, et al. Prostate cancer: local staging at 3-T endorectal MR imaging—early experience. Radiology 2006;238(1):184–191.

97. Engelbrecht MR, Jager GJ, Laheij RJ, Verbeek AL, van Lier HJ, Barentsz JO. Local staging of prostate cancer using magnetic resonance imaging: a meta-analysis. Eur Radiol 2002;12(9):2294–2302.

98. Fütterer JJ, Engelbrecht MR, Jager GJ, et al. Prostate cancer: comparison of local staging accuracy of pelvic phased-array coil alone versus integrated endorectal-pelvic phased-array coils. Local staging accuracy of prostate cancer using endorectal coil MR imaging. Eur Radiol 2007;17(4): 1055–1065.

99. Tempany CM, Zhou X, Zerhouni EA, et al. Staging of prostate cancer: results of Radiology Diagnostic Oncology Group project comparison of three MR imaging techniques. Radiology 1994;192(1):47–54.

100. Augustin H, Fritz GA, Ehammer T, Auprich M, Pummer K. Accuracy of 3-Tesla magnetic resonance imaging for the staging of prostate cancer in comparison to the Partin tables. Acta Radiol 2009;50(5):562–569.

101. Chandra RV, Heinze S, Dowling R, Shadbolt C, Costello A, Pedersen J. Endorectal magnetic resonance imaging staging of prostate cancer. ANZ J Surg 2007;77(10):860–865.

102. Heijmink SW, Fütterer JJ, Hambrock T, et al. Prostate cancer: body-array versus endorectal coil MR imaging at 3 T—comparison of image quality, localization, and staging performance. Radiology 2007; 244(1):184–195.

103. Porcaro AB, Migliorini F, Monaco C, et al. Accuracy of magnetic resonance imaging with endorectal coil (ER-MRI) in staging early prostate cancer (EPC) before radical prostatectomy (RP). Eur Urol Suppl 2009; 8(4):355.

104. Torricelli P, Barberini A, Cinquantini F, Sighinolfi M, Cesinaro AM. 3-T MRI with phased-array coil in local staging of prostatic cancer. Acad Radiol 2008;15(9):1118–1125.

105. Latchamsetty KC, Borden LS Jr, Porter CR, et al. Experience improves staging accuracy of endorectal magnetic resonance imaging in prostate cancer: what is the learning curve? Can J Urol 2007;14(1):3429–3434.

106. Bloch BN, Furman-Haran E, Helbich TH, et al. Prostate cancer: accurate determination of extracapsular extension with high-spatial-resolution dynamic contrast-enhanced and T2-weighted MR imaging—initial results. Radiology 2007;245(1): 176–185.

107. Lee SH, Park KK, Choi KH, et al. Is endorectal coil necessary for the staging of clinically localized prostate cancer? Comparison of non-endorectal versus endorectal MR imaging. World J Urol 2010;28(6): 667–672.

108. Beyersdorff D, Taymoorian K, Knösel T, et al. MRI of prostate cancer at 1.5 and 3.0 T: comparison of image quality in tumor detection and staging. AJR Am J Roentgenol 2005;185(5):1214–1220.

109. Park BK, Kim B, Kim CK, Lee HM, Kwon GY. Comparison of phased-array 3.0-T and endorectal 1.5-T magnetic resonance imaging in the evaluation of local staging accuracy for prostate cancer. J Comput Assist Tomogr 2007;31(4):534–538.

110. Fütterer JJ, Engelbrecht MR, Huisman HJ, et al. Staging prostate cancer with dynamic contrast-enhanced endorectal MR imaging prior to radical prostatectomy: experienced versus less experienced readers. Radiology 2005;237(2):541–549.

111. Yu KK, Scheidler J, Hricak H, et al. Prostate cancer: prediction of extracapsular extension with endorectal MR imaging and three-dimensional proton MR spectroscopic imaging. Radiology 1999;213(2):481–488.

112. Masterson TA, Touijer K. The role of endorectal coil MRI in preoperative staging and decision-making for the treatment of clinically localized prostate cancer. MAGMA 2008;21(6):371–377.

113. Gleason DF, Mellinger GT. Prediction of prognosis for prostatic adenocarcinoma by combined histological grading and clinical staging. J Urol 1974;111(1):58–64.

114. Epstein JI, Allsbrook WC Jr, Amin MB, Egevad LL; ISUP Grading Committee. The 2005 International Society of Urological Pathology (ISUP) Consensus Conference on Gleason Grading of Prostatic Carcinoma. Am J Surg Pathol 2005;29(9):1228–1242.

115. Ruijter E, van Leenders G, Miller G, Debruyne F, van de Kaa C. Errors in histological grading by prostatic needle biopsy specimens: frequency and predisposing factors. J Pathol 2000;192(2):229–233.

116. Ikonen S, Kärkkäinen P, Kivisaari L, et al. Magnetic resonance imaging of prostatic cancer: does detection vary between high and low Gleason score tumors? Prostate 2000;43(1):43–48.

117. Shukla-Dave A, Hricak H, Ishill NM, et al. Correlation of MR imaging and MR spectroscopic imaging findings with Ki-67, phospho-Akt, and androgen receptor expression in prostate cancer. Radiology 2009;250(3):803–812.

118. Zakian KL, Sircar K, Hricak H, et al. Correlation of proton MR spectroscopic imaging with Gleason score based on step-section pathologic analysis after radical prostatectomy. Radiology 2005;234(3):804–814.

119. Kurhanewicz J, Swanson MG, Nelson SJ, Vigneron DB. Combined magnetic resonance imaging and spectroscopic imaging approach to molecular imaging of prostate cancer. J Magn Reson Imaging 2002;16(4): 451–463.

120. Kobus T, Hambrock T, Hulsbergen-van de Kaa CA, et al. In Vivo Assessment of Prostate Cancer Aggressiveness Using Magnetic Resonance Spectroscopic Imaging at 3 T with an Endorectal Coil. Eur Urol 2011 Mar 16. [Epub ahead of print]

121. Verma S, Rajesh A. A clinically relevant approach to imaging prostate cancer: self-assessment module. AJR Am J Roentgenol 2011;196(3 Suppl):S11–S14.

122. Warlick C, Trock BJ, Landis P, Epstein JI, Carter HB. Delayed versus immediate surgical intervention and prostate cancer outcome. J Natl Cancer Inst 2006;98(5): 355–357.

123. Freedland SJ, Kane CJ, Amling CL, et al. Delay of radical prostatectomy and risk of biochemical progression in men with low risk prostate cancer. J Urol 2006;175(4): 1298–1302; discussion 1302–1303.

124. Dall'Era MA, Cooperberg MR, Chan JM, et al. Active surveillance for early-stage prostate cancer: review of the current literature. Cancer 2008;112(8):1650–1659.

125. Roemeling S, Roobol MJ, de Vries SH, et al. Active surveillance for prostate cancers detected in three subsequent rounds of a screening trial: characteristics, PSA doubling times, and outcome. Eur Urol 2007; 51(5):1244–1250; discussion 1251.

126. Klotz L, Zhang L, Lam A, Nam R, Mamedov A, Loblaw A. Clinical results of long-term follow-up of a large, active surveillance cohort with localized prostate cancer. J Clin Oncol 2010;28(1):126–131.

127. Carter HB, Kettermann A, Warlick C, et al. Expectant management of prostate cancer with curative intent: an update of the Johns Hopkins experience. J Urol 2007;178(6):2359–2364; discussion 2364–2365.

128. Berglund RK, Masterson TA, Vora KC, Eggener SE, Eastham JA, Guillonneau BD. Pathological upgrading and up staging with immediate repeat biopsy in patients eligible for active surveillance. J Urol 2008;180(5):1964–1967; discussion 1967–1968.

129. Giles SL, Morgan VA, Riches SF, Thomas K, Parker C, deSouza NM. Apparent diffusion coefficient as a predictive biomarker of prostate cancer progression: value of

fast and slow diffusion components. AJR Am J Roentgenol 2011;196(3):586–591.

130. van As NJ, de Souza NM, Riches SF, et al. A study of diffusion-weighted magnetic resonance imaging in men with untreated localised prostate cancer on active surveillance. Eur Urol 2009;56(6):981–987.

131. Fradet V, Kurhanewicz J, Cowan JE, et al. Prostate cancer managed with active surveillance: role of anatomic MR imaging and MR spectroscopic imaging. Radiology 2010;256(1):176–183.

132. Cabrera AR, Coakley FV, Westphalen AC, et al. Prostate cancer: is inapparent tumor at endorectal MR and MR spectroscopic imaging a favorable prognostic finding in patients who select active surveillance? Radiology 2008;247(2):444–450.

133. Tamada T, Sone T, Jo Y, et al. Apparent diffusion coefficient values in peripheral and transition zones of the prostate: comparison between normal and malignant prostatic tissues and correlation with histologic grade. J Magn Reson Imaging 2008; 28(3):720–726.

134. Tanimoto A, Nakashima J, Kohno H, Shinmoto H, Kuribayashi S. Prostate cancer screening: the clinical value of diffusion-weighted imaging and dynamic MR imaging in combination with T2-weighted imaging. J Magn Reson Imaging 2007;25(1): 146–152.

135. Ren J, Huan Y, Wang H, et al. Diffusion-weighted imaging in normal prostate and differential diagnosis of prostate diseases. Abdom Imaging 2008;33(6):724–728.

136. Mazaheri Y, Shukla-Dave A, Hricak H, et al. Prostate cancer: identification with combined diffusion-weighted MR imaging and 3D 1H MR spectroscopic imaging—correlation with pathologic findings. Radiology 2008;246(2):480–488.

137. Reinsberg SA, Payne GS, Riches SF, et al. Combined use of diffusion-weighted MRI and 1H MR spectroscopy to increase accuracy in prostate cancer detection. AJR Am J Roentgenol 2007;188(1):91–98.

138. Gibbs P, Pickles MD, Turnbull LW. Diffusion imaging of the prostate at 3.0 tesla. Invest Radiol 2006;41(2):185–188.

139. Pickles MD, Gibbs P, Sreenivas M, Turnbull LW. Diffusion-weighted imaging of normal and malignant prostate tissue at 3.0T. J Magn Reson Imaging 2006;23(2):130–134.